CHALMERS

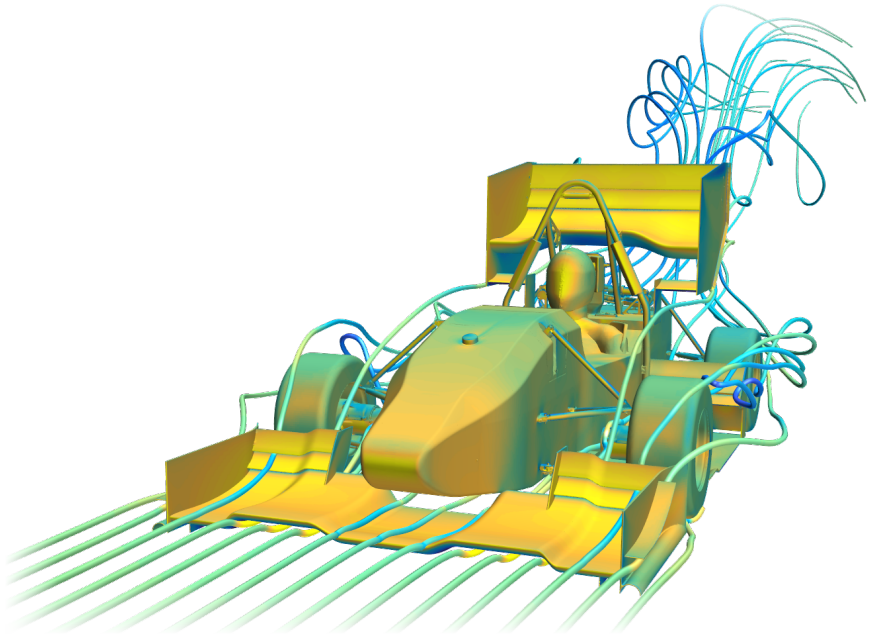

Development and performance evaluation of undertray diffusers during racing manuevers

Bachelor's thesis in Mechanics and Maritime Sciences

WILLEM DE WILDE
JACOB GUNNARSSON
LENA IVARSSON
LINNÉUS KARLSSON
OSKAR KOLTE
DANIEL OLANDER

DEPARTMENT OF MECHANICS AND MARITIME SCIENCES

CHALMERS UNIVERSITY OF TECHNOLOGY
Gothenburg, Sweden 2021
www.chalmers.se

Bachelor's thesis 2021:12

Development and performance evaluation of undertray diffusers during racing manuevers

WILLEM DE WILDE
JACOB GUNNARSSON
LENA IVARSSON
LINNÉUS KARLSSON
OSKAR KOLTE
DANIEL OLANDER

Department of Mechanics and Maritime Sciences
Division of Vehicle Engineering and Autonomous Systems
Chalmers University of Technology
Gothenburg, Sweden 2021

Development and performance evaluation of undertray diffusers during racing manuevers

WILLEM DE WILDE
JACOB GUNNARSSON
LENA IVARSSON
LINNÉUS KARLSSON
OSKAR KOLTE
DANIEL OLANDER

Supervisor: Erik Josefsson, Division of Vehicle Engineering and Autonomous Systems
Examiner: Simone Sebben, Division of Vehicle Engineering and Autonomous Systems

Bachelor's Thesis 2021
Department of Mechanics and Maritime Sciences
Chalmers University of Technology
SE-412 96 Gothenburg
Telephone +46 31 772 1000

Cover: Velocity streamlines around the Chalmers Formula Student car and C_p visualized on the surface while driving straight.

Typeset in LaTeX
Printing /Department of Mechanics and Maritime Sciences
Gothenburg, Sweden 2021

Abstract

A potential to develop the monocoque and diffuser on the Chalmers Formula Student (CFS) car, as to increase its downforce, was identified by CFS. Downforce is the downward aerodynamic lifting force that is obtained when a pressure difference is created between the top and bottom of the car. This effect is crucial for the grip of the car in driving scenarios like cornering, accelerating and braking. With more downforce, accelerating and braking can be done faster, and higher speeds can be maintained in cornering.

The objective of this project is to develop a methodology for modeling of aerodynamic forces during different racing maneuvers of a CFS car. These new methods are purely computational. Further, the methods are used in the development of a new diffuser concept. This is done with the aim of providing CFS with knowledge and proof-of-concept of the implementation of a new diffuser, which could increase aerodynamic performance of the car.

It was shown that straight ahead driving, braking, and cornering were the most critical driving scenarios. These were used to perform three types of simulations. Different diffuser designs were simulated based on these scenarios. It was further shown that the following parameters had an effect on aerodynamic performance: the expansion angle of the diffuser, the starting point of the diffuser, the radius of the diffuser throat, and the implementation of strakes and side floors. Differences in the performance robustness of the different designs were observed.

Two diffusers provided the greatest downforce: one with a 13° expansion angle and the other with a 19° expansion angle. The diffusers were in other regards identical. Lastly, the 13° diffuser was chosen as the best contending design, due to its robust performance in each of the simulated driving scenarios.

Keywords: CFD, aerodynamics, Formula Student, downforce, lift coefficient, drag coefficient, diffuser, racing manuevers, cornering, braking.

Sammandrag

En potential att vidareutveckla monocoque och diffusor på Chalmers Formula Student-bilen (CFS-bilen), med avsikt att öka bilens downforce, identifierades av CFS. Downforce kallas den nedåtriktade aerodynamiska lyftkraft, som uppstår vid en tryckskillnad mellan bilens ovan- och undersida. Denna effekt är avgörande för bilens grepp i körscenarier såsom kurvtagning, acceleration och inbromsning. Större downforce tillåter kraftigare acceleration och inbromsning och att högre hastighet kan hållas under kurvtagning.

Detta projekts syfte är att utveckla en metodik för att modellera aerodynamiska krafter under de olika manövrar som en CFS-bil gör under en tävling. Dessa metoder är baserade på simuleringar. Vidare ska metoderna användas för att assistera utvecklingen av ett nytt diffusor-koncept. Detta görs med målet att tillhandahålla CFS kunskap om, och konceptvalidering för implementeringen av en ny diffusor, vilket kan förbättra bilens aerodynamiska prestanda.

Det visades att rak körning, inbromsning och kurvtagning var de mest kritiska körscenarierna. Tre typer av simulering baserades på dessa scenarier. Olika typer av diffusorer undersöktes med dessa simuleringstyper. Vidare visades att följande parametrar hade en inverkan på bilens prestanda: diffusorns expansionsvinkel, diffusorns övergångsradie, samt implemetering av skiljeväggar och sidogolv. Skillnader i de olika diffusorernas prestandas robusthet observerades.

Två diffusorer genererade störst downforce: en med expansionsvinkeln 13°, och den andra med expansionsvinkeln 19°. I andra hänseenden var diffusorerna identiska. Slutligen valdes diffusorn med 13° expansionsvinkel som den bäst presterande av de undersökta. Detta baserades på dess robusta prestanda i alla undersökta körscenarier.

Nyckelord: CFD, aerodynamik, Formula Student, downforce, lyftkraftskoefficient, motståndskoefficient, diffusor, manövrar, kurvtagning, inbromsning.

Acknowledgements

We would like to express our greatest gratitude to our supervisor Erik Josefsson, Ph.D student in the Road Vehicle Aerodynamics research group, for all the help and guidance throughout this bachelor thesis.

We would also like to thank Simone Sebben, professor in Aerodynamics and manager of the division Vehicle Engineering and Autonomous Systems, for the opportunity to carry out this thesis. Simone Sebben has given us lectures that have been very useful in the project.

Finally we would like to thank the Chalmers Formula Student 2021 team for their cooperation. We are particularly grateful for Christian Svensson's invaluable source of knowledge and willingness to help in this project.

The authors, Gothenburg, May 2021

Contents

Nomenclature and Abbreviations

Fluid Mechanics

μ	Dynamic viscosity [$\mathrm{kg} \cdot \mathrm{m} \cdot \mathrm{s}^{-1}$]
ν	Kinematic viscosity [$\mathrm{m}^2 \cdot \mathrm{s}^{-1}$]
ρ	Density [$\mathrm{kg} \cdot \mathrm{m}^{-3}$]
τ	Shear stress [$\mathrm{N} \cdot \mathrm{m}^{-2}$]
τ_w	Wall shear stress [$\mathrm{N} \cdot \mathrm{m}^{-2}$]
$\vec{\zeta}$	Flow vorticity vector [s^{-1}]
$\vec{u}$	Flow velocity vector[$\mathrm{m} \cdot \mathrm{s}^{-1}$]
C_D	Coefficient of drag [-]
C_f	Coefficient of skin friction [-]
C_L	Coefficient of lift in the direction of -$\hat{z}$ [-]
C_p	Coefficient of pressure [-]
F_D	Drag force [N]
F_L	Lift force [N]
p	Static pressure [Pa]
p_∞	Freestream flow pressure [Pa]
u	Flow velocity in x-direction or $\lvert\vec{u}\rvert$ [$\mathrm{m} \cdot \mathrm{s}^{-1}$]
u_∞	Freestream flow velocity [$\mathrm{m} \cdot \mathrm{s}^{-1}$]
V	Volume [m^3]
v	Flow velocity in y-direction [$\mathrm{m} \cdot \mathrm{s}^{-1}$]
w	Flow velocity in z-direction [$\mathrm{m} \cdot \mathrm{s}^{-1}$]
y^+	Dimensionless distance from wall [-]
Re	Reynolds number [-]

Vehicle Dynamics

$\hat{x}$	Coordinate axis pointing towards the rear of the car
$\hat{y}$	Coordinate axis pointing towards the right side of the car
$\hat{z}$	Coordinate axis pointing upwards

Other Symbols

g	Gravitational acceleration [$\mathrm{m} \cdot \mathrm{s}^{-2}$]

Abbreviations

CAD	Computer-aided Design
CFD	Computational Fluid Dynamics
CFS	Chalmers Formula Student
COG	Center Of Gravity
COP	Center Of Pressure
FS	Formula Student
FVM	Finite Volume Method

M&D Monocoque and Diffuser
SNIC Swedish National Infrastructure for Computing

Software

CATIA V5 Software package for CAD
MATLAB Mathematical software used for calculations and data analysis
Simcenter Star-CCM+ Software used for simulations in CFD

List of Figures

List of Tables

1
Introduction

Formula Student (FS) is a competition where universities and engineering students design and build formula cars. Chalmers team is called Chalmers Formula Student (CFS) and has been building electric formula cars since 2015. The average speed in competition for a Formula Student car is about 50 km/h, while the top speed is about 110 km/h [1]. The current CFS car has a diffuser, but it is believed that there is great potential in improving the flow around the floor and the diffuser to create more downforce.

Downforce is a force that refers to the downward aerodynamic lifting force that is obtained on a car when a pressure difference is created between the top and bottom of the car. As downforce increases in a racing car, the tires generate more friction, which results in increased grip against the ground. This means that the car can accelerate more without the wheels spinning and that higher speeds can be maintained in corners. A diffuser is an aerodynamic part belonging to the bodywork at the rear of the car, see Figure 1.1. By applying a diffuser, the pressure under the car can decrease in relation to the pressure above the car thus generating more downforce. A diffuser also plays an important role in returning the air flow under the car to the ambient air in a smooth way to minimize energy losses, reducing the drag.

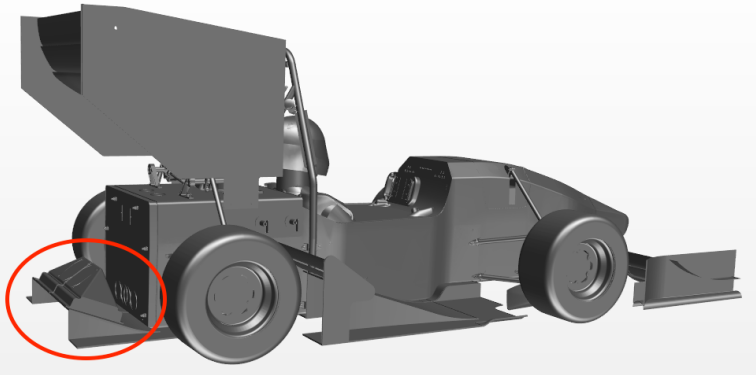

Figure 1.1: 3D representation of the CFS21 car. The diffuser is marked in red.

Different dynamic driving scenarios such as cornering, braking and acceleration affect how well all the car's aerodynamic components (aero package) work. The airflow when the car is driving straight ahead at a constant speed does not interact with the car in the same way as when the car is cornering. Thus, the pressure distribution

and consequently the downforce in the two cases differ. For a formula car, downforce is most critical in dynamic driving scenarios where the car's grip is most important. Implementation of different dynamic driving scenarios in aerodynamic simulations has rarely been done by the CFS team. However, this is something the team believe will bring benefits for future aerodynamic development. A structured method for modeling of such dynamic scenarios would be favorable for the 2021/2022 CFS team (CFS22) and future CFS teams.

1.1 Historical Background

Motorsport began developing in the end of the 19th century following the invention of the petrol fueled internal-combustion engine. Until 1960, the development of racing cars consisted mainly of strengthening the engines and generating more grip by developing chassis and wheel suspension. This required costly investments, which led to only the largest manufacturers being able to afford continued development and thus the opportunity to fight for a top position during competition. For the smaller manufacturers, new cheaper development areas were therefore needed, and the development of aerodynamics came into focus. Previously, the development of car aerodynamics had been intended to reduce air resistance, but in the late 1960s, motorsport engineers observed that downforce was also important for faster cornering. This led to innovative designs of cars that used downforce, which resulted in drastically improved lap times. Since then, aerodynamics has played a central role in motorsports [2].

In Formula 1, in particular, aerodynamic improvements have been of great importance. With increased knowledge about aerodynamics, higher speeds can be maintained, but also lower fuel consumption, lower wind noise and higher comfort are achieved. In the late 60's, the first F1 car with a front wing and a rear spoiler, the Lotus 49B, was presented. During this period experiments of having wings high above the body of the car were carried out on, for example, the Matra MS10. Since the 60's, lots of technical innovations in aerodynamics have been tested. Among other things, skirts have been added to the body work, in order to get the maximum ground effect. Lots of different wing and underbody designs have also been tested [3]. One of the most radical F1 cars of all time was the Brabham BT46B, also known as the "fan car". The car was designed by Gordon Murray and was equipped with a large fan that generated an immense amount of downforce by extracting air from the underside of the car. The car only raced once at the Swedish Grand Prix in Anderstorp in 1978, where the car also won before the concept was withdrawn [4]. It is still an ongoing process for motorsport engineers to look for areas for aerodynamic improvement in order to find that little extra performance that is crucial in a race.

1.2 Objective

The objective of this project is to develop a methodology for modeling of aerodynamic forces during different racing maneuvers of a CFS car. These new methods

will then be used in the development of a new diffuser concept. This is done with the aim of providing CFS with knowledge and proof-of-concept of the implementation of a new diffuser, which could increase aerodynamic performance of the car.

1.3 Working Methods

The modeling of aerodynamic forces on the CFS car has been done using Computational Fluid Dynamics (CFD). Setups for relevant driving scenarios such as driving straight ahead, cornering and braking were simulated using a range of new diffuser design concepts. This was done in order to draw conclusions of how well a design concept works in dynamic driving scenarios, i.e. how aerodynamically robust it is.

Design concepts were developed using 3D Computer Aided Design (CAD). A base model of the CFS21 car was obtained from CFS and used as a baseline. Iterations of a new diffuser concept were systematically developed and simulated using CFD. Furthermore, CFS shared three post-processing scripts. These were edited and used to produce necessary data and plots to analyze the simulations.

1.4 Delimitations

The project is delimited in several regards. For instance the diffuser concepts developed in the project will not be manufactured. It will only be visualized in three dimensional CAD, and simulated using CFD.

When developing a new diffuser, the design is based on the rules for Formula Student in 2022 [5]. However, the regulations tend to look different from year to year when it comes to powered aero devices such as fans, which is the reason for the project to develop a diffuser design that performs good even without fans. Should it be of interest to add fans, then it should be for the purpose of tuning an already good performance. Hence the project is based on a diffuser without fans.

In an aerodynamic package of a formula car, the aerodynamic components interacts in complex and often unpredictable ways with each other. Because of this complexity and the project's limited time and computational resources, it is necessary to have practical limitation of how in-depth the work can be. Therefore, the design development will only be focused on the diffuser. Design of other parts of the car's aero package will thus not be covered in this project.

The project also does not include any mesh study. Mesh studies aim, among other things, to ensure convergence and independence of mesh for the solution in the simulation. Instead of doing a mesh study, CFS current mesh was used with some refinements since CFS has already performed one [6]. More about the refinements are mentioned in Section 3.2.

Only CFD simulations will be performed in order to analyze the aerodynamics of

the formula car, an thus no wind tunnel experiments. Due to the fact that no wind tunnel experiments will be carried out, no validation will be made in the form of correlation between simulations in CFD and wind tunnel testing. This will not be possible due to, among other things, that no diffuser will be manufactured. Wind tunnel experiments are also resource and time consuming.

Assumptions of stationary flow is made for all simulations in the project. This means that the car's position and quantities, such as velocity and pressure, don't change with time. This assumption is done due to the fact that non-stationary flow would be too time consuming to base the simulations on. Thermodynamic effects on the flow are not taken into account in the project either. This is because its impact is considered to have a relatively insignificant impact on this project.

The project will primarily focus on generating as high downforce as possible. Drag force is of secondary priority. Downforce always comes with the penalty of increased dragforce. However, in Formula Student it has been shown that increased downforce results in faster lap times almost regardless of any realistic drag force penalty [7]. This is true up to a factor of $\Delta C_D/\Delta C_L = 3$, where ΔC_D is a unit of gained drag coefficient (see Section 2.1.2.2) and ΔC_L a unit of gained lift coefficient (see Section 2.1.2.3), as shown by previous CFS team members.

No major consideration is given to the packaging of electronic components when designing the diffuser. When testing how early a diffuser concept can begin, parts of the electronics and battery storage are cut off. However, a plausibility assessment is made in order to decide how much of the electronics can be moved in order to let the diffuser start earlier.

2
Theory

In this chapter, the fundamental physics phenomena which are central to the project are described. Further, the working principles of an undertray diffuser are investigated.

2.1 Fundamental Fluid Dynamics Theory

The relevant portion of fundamental fluid dynamics theory is presented in this section. These principles are relevant to describe aerodynamics as a subject. In addition, most of them are utilized by the CFD program Star-CCM+ which is further described in Section 3.2. The presented variables are described in Nomenclature.

2.1.1 Bernoulli's Principle and the Continuity Equation

In incompressible isentropic flow, i.e. a flow where a negligible amount of energy is lost to non-reversible processes such as heat in turbulent flows, one can derive Bernoulli's principle from the conservation of energy

$$\frac{u^2}{2} + \frac{p}{\rho} + z \cdot g = constant, \tag{2.1}$$

where z is the vertical position of a fluid element. This law states that an increase in velocity implies a decrease in pressure and vice versa. This is the working principle for wing profiles and diffusers [8].

Further, the continuity equation for mass flow provides a relationship between flow area in a closed channel and flow velocity

$$\frac{\partial \rho}{\partial t} + \rho \boldsymbol{\nabla} \cdot \vec{u} = 0 \implies A_{\text{flow}} \cdot u = \frac{\dot{m}}{\rho} = constant, \tag{2.2}$$

where A_{flow} represents the swept area of the fluid flow, t time and $\dot{m}$ the mass flow rate through A_{flow}.

2.1.2 Dimensionless parameters

Dimensionless parameters are used to make a parameter comparable with parameters of other types of flow. Below the relevant parameters are presented.

2.1.2.1 Reynolds Number

The Reynolds number, Re, is a dimensionless number which tells the relation between the inertia and viscosity in a newtonian fluid and is defined as

$$\mathrm{Re} = \frac{\rho V L}{\mu} = \left\{ \frac{\text{Inertia}}{\text{Viscosity}} \right\} \tag{2.3}$$

V and L are the characteristic velocity and length of the flow. A high Re is associated with a fast, large-scale turbulent flow, whereas a low Re corresponds to a slow, viscous flow. Fast flows of gas imply a relatively high Re [8].

2.1.2.2 Drag Coefficient, C_D

The drag coefficient of a body, C_D, is a dimensionless number indicative of drag force. C_D is defined as

$$C_D = \frac{F_D}{\frac{1}{2}\rho u_\infty^2 A}, \tag{2.4}$$

where A is the projected area from the front of the body and the denominator ($\frac{1}{2}\rho u_\infty^2$) is the dynamic pressure of the free stream [8].

2.1.2.3 Lift Coefficient, C_L

The lift coefficient of a body, C_L is defined as

$$C_L = \frac{F_L}{\frac{1}{2}\rho u_\infty^2 A}, \tag{2.5}$$

where A is projected area from the front of the body. C_L is a dimensionless coefficient that increases with lift force [8]. In this study, C_L will indicate the lift in negative $\hat{z}$-direction, i.e. a high downforce will correspond to a large C_L.

2.1.2.4 Pressure Coefficient, C_p

The pressure coefficient , C_p, is a dimensionless parameter that describes the relative pressure. C_p is defined as

$$C_p = \frac{p - p_\infty}{\frac{1}{2}\rho u_\infty^2}, \tag{2.6}$$

where p is the static pressure at the point where C_p is calculated, while p_∞ is the static pressure in the free stream [8].

2.1.2.5 Skin Friction Coefficient, C_f

The skin friction coefficient, C_f, is a dimensionless parameter defined as [8]

$$C_f = \frac{\tau_w}{\frac{1}{2}\rho u_\infty^2}. \tag{2.7}$$

2.1.3 Vorticity

The vorticity, $\vec{\zeta}$, is defined as the curl of the velocity field, $\nabla \times \vec{u}$, which relates to the rotation of a velocity field. If the vorticity is zero the flow has no rotation and is called irrotational [8]. The voriticity in x direction is given by

$$\zeta_x = \frac{\partial w}{\partial y} - \frac{\partial v}{\partial z}. \tag{2.8}$$

2.1.4 Navier-Stokes Equations

A fluid can be described with the Navier-Stokes equations if it is incompressible and newtonian [8] as

$$\rho\left(\frac{\partial \vec{u}}{\partial t} + (\vec{u}\cdot\nabla)\vec{u}\right) = \rho\vec{g} - \nabla p + \mu\Delta\vec{u}. \tag{2.9}$$

2.1.5 RANS

In turbulent flow there are fluctuations that causes rapid changes in the velocity and pressure in the Navier-stokes equations (Eq. 2.9). These rapid changes can be easier to account for if the velocity and pressure are split into a mean variable $\bar{u}$ and a fluctuation variable u'. The velocity in the x-direction is therefore $u = \bar{u}+u'$. If those splits is put into the Navier-stokes equations we get the Reynold's Averaged Navier Stokes (RANS) equations after some derivations [8]. The RANS in x-direction is

$$\rho\frac{d\overline{u}}{dt} = -\frac{\partial\overline{p}}{\partial x} + \rho g_x + \frac{\partial}{\partial x}\left(\mu\frac{\partial\overline{u}}{\partial x} - \rho\overline{u'^2}\right) + \frac{\partial}{\partial y}\left(\mu\frac{\partial\overline{u}}{\partial y} - \rho\overline{u'v'}\right) + \frac{\partial}{\partial z}\left(\mu\frac{\partial\overline{u}}{\partial z} - \rho\overline{u'w'}\right). \tag{2.10}$$

2.1.6 Flow Past Boundary

Bodies, such as plates, immersed in a fluid stream create a boundary layer flow. The boundary layer is defined as the region where the flow velocity is less than 99 percent of the velocity of the external flow (u_∞). The boundary layer flow is made up of two parts, the laminar part and the turbulent part:

$$\frac{\delta}{x} \approx \begin{cases} \dfrac{5}{\mathrm{Re}_x^{1/2}} & 10^3 < \mathrm{Re}_x < 10^6 \text{ laminar flow} \\ \dfrac{0.16}{\mathrm{Re}_x^{1/7}} & 10^6 < \mathrm{Re}_x \text{ turbulent flow} \end{cases}. \tag{2.11}$$

δ is the thickness of the boundary layer and Re_x the Reynolds number at x [8]. An illustration of he boundary level flow can be seen in Figure 2.1.

2.1.6.1 Flow Separation

Backflow, i.e. flow going in the opposite direction of the freestream, at the wall indicates that the flow is separated. The point of separation is when the wall shear is 0 which means the velocity gradient is 0 [8].

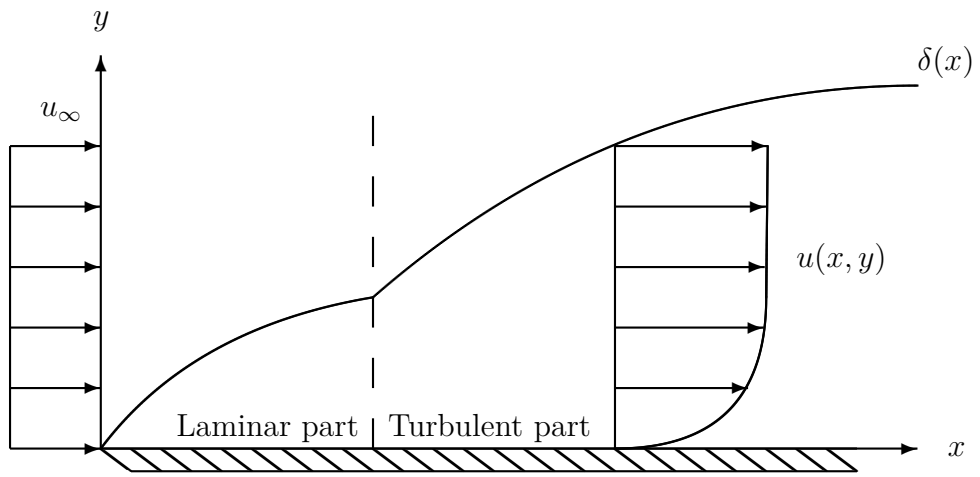

Figure 2.1: Flow close to a wall. The flow enters and acts laminar and then changes and becomes turbulent at $\mathrm{Re}_x > 10^6$.

2.1.6.2 The Logarithmic Overlap Law

The turbulent flow near a wall can be broken up in three regions based on which shear stress dominates:

- Wall layer: Viscous shear dominates.
- Outer layer: Turbulent shear dominates.
- Overlap layer: A mix of the shear types.

We define the dimensionless number y^+ as

$$y^+ = \frac{yu^*}{\nu}, \tag{2.12}$$

where $u^* = \sqrt{\tau_w/\rho}$. For $y^+ \in [0, 5]$ the inner layer dominates and is proportional to y^+. It can be described with the dimensionless variable

$$u^+ = \frac{u}{u^*} = y^+. \tag{2.13}$$

For $y^+ \in [30, 10^3]$ the overlap layers dominates and can be described as

$$u^+ = \frac{1}{\kappa} \ln y^+ + B, \tag{2.14}$$

where $\kappa \approx 0.41$ and $B \approx 5.0$. For $y^+ \in [5, 30]$ the inner layer has to curve so it merges with the overlap layer. Only experimental data exists for this interval making it difficult to model [8].

2.2 CFD Theory

Numerically solving the equations that describe the airflow around the car is a complex process. It is important to determine the accuracy needed in the simulation to arrive at a balance of the resources needed for the simulation and its accuracy. Different mathematical models for the modeling of the flow can be used. These models have their respective strengths and weaknesses, and should be chosen with care. This requires a basic understanding of key concepts in CFD simulation.

2.2.1 Finite Volume Method

The Finite Volume Method (FVM) is a numerical method used to solve the partial differential equations encountered in fluid mechanics. The first step in the FVM is to discretize the domain of interest into a finite amount of control volumes (cells). The variables of interest are located at the centroid of these cells. The second step is integration of the governing equations over the cell to solve for these variables. Lastly, interpolation profiles are assumed between cell centroids in order to describe the variation of the variables of interest [9].

2.2.2 The $k - \epsilon$ Turbulence Model

$k-\epsilon$ is a type of RANS turbulence model that can be used in CFD. The $k-\epsilon$ model solves the equations for k and ϵ where k is the turbulent kinetic energy and ϵ the rate of dissipation. $k - \epsilon$ is accurate around external flow problems but not very accurate in complex curves. The model is fast and has a good convergence rate [10].

2.2.3 The $k - \omega$ Turbulence Model

$k - \omega$ is likewise the $k - \epsilon$ model a type of RANS turbulence model . The $k - \omega$ model solves the equations for k and ω where k is the turbulent kinetic energy and ω is the specific dissipation rate. Contrary to the $k - \epsilon$ method, the $k - \omega$ method is especially accurate in internal flow, flow past complex curvature and in separated flow. The method is more complex than the $k - \epsilon$ model which leads to it being slower and more difficult to converge [10].

2.2.4 The SST $k - \omega$ Model

The SST $k-\omega$ model is a mixup of the $k-\omega$ method and the $k-\epsilon$ method where SST is Shear Stress Transport. Since the $k - \omega$ method is better near walls it influences the result near the walls and because it's not very good in the free stream there is a transition from the $k - \omega$ method to the $k - \epsilon$ method in the free stream [11].

2.3 Vehicle Dynamics Theory

In this section, vehicle dynamics parameters relevant to this study are described. Furthermore, aerodynamic influence on vehicle dynamics in relation to these param-

eters are discussed in this section.

2.3.1 Steering Angle

The steering angle is the angle between the direction of a wheel and the car's longitudinal axis. The steering angle for each front wheel can be different if the car has Ackermann steering [12]. An illustration can be found in Figure 2.2.

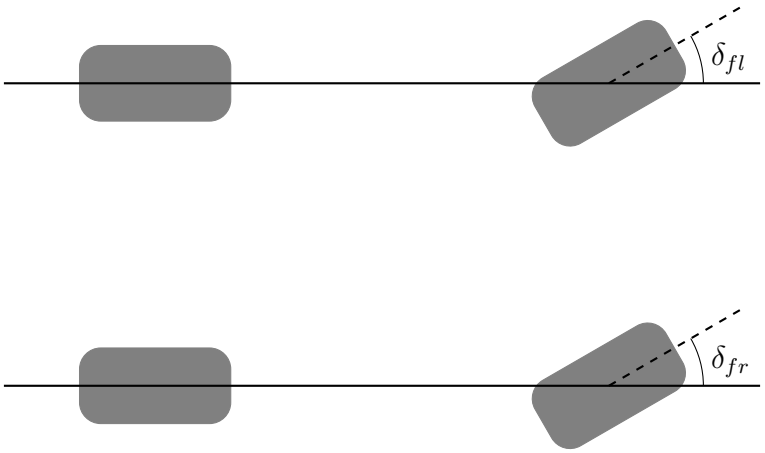

Figure 2.2: Steering angles, δ_{fl} for the left wheel and δ_{fr} for the right wheel. These angles can differ from each other if the car has Ackermann steering.

2.3.2 Body Slip Angle

The body slip angle is an yaw angle meaning it is the angle that is created when the car rotates around its vertical axis. The rotational axis goes through the car's center of gravity. The body slip angle is the angle between the velocity vector of the car and the car's longitudinal direction [12]. A visual representation of the body slip angle can be seen in Figure 2.3.

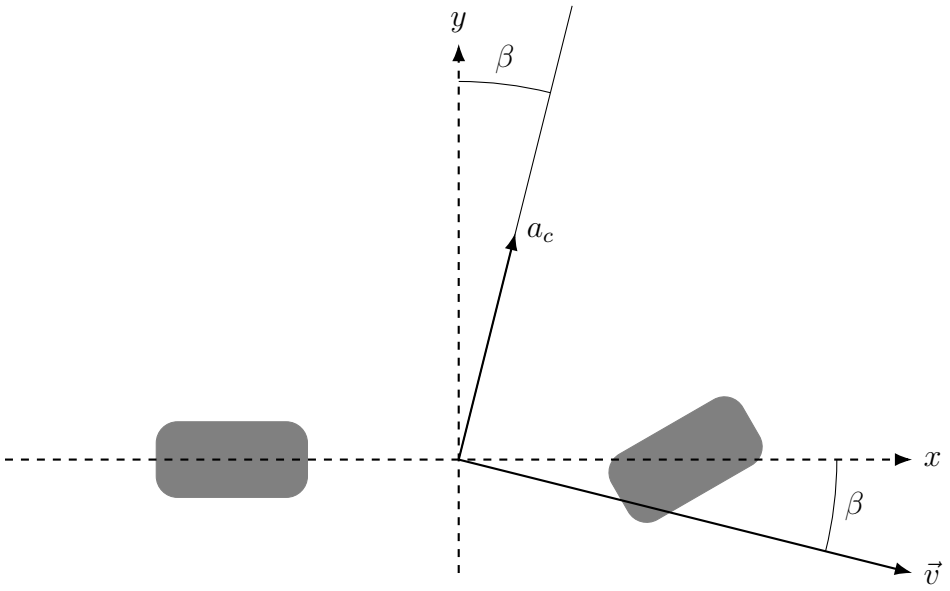

Figure 2.3: A body slip angle β. The car's longitudinal direction is pointing in the x direction while it is moving in a different direction $\vec{v}$ thus creating a slip angle β. The centripetal acceleration a_c is acting on the car's center of mass towards the corner's center.

2.3.3 Pitch Angle

The pitch angle is the angle that is created if the vehicle's sprung mass (everything but the wheels) rotates around its lateral axis which is shown in Figure 2.4. The vehicle rotates around what is called its pitch center [12].

Figure 2.4: A pitch angle θ around the car's lateral axis.

2.3.4 Roll Angle

The roll angle is the angle that is created if the vehicle's sprung mass rotates around its longitudinal axis, see Figure 2.5. The vehicle rotates around what is called its roll center [12].

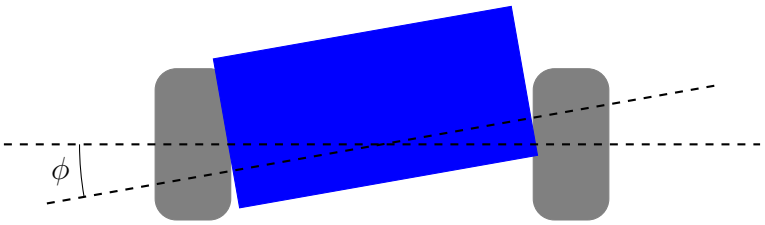

Figure 2.5: A roll angle ϕ around the car's longitudinal axis.

2.3.5 Ride Height

The ride height is the smallest distance between the ground and the car's floor when it is stationary, see Figure 2.6. For a Formula Student car the ride height must at least be 30 mm [5].

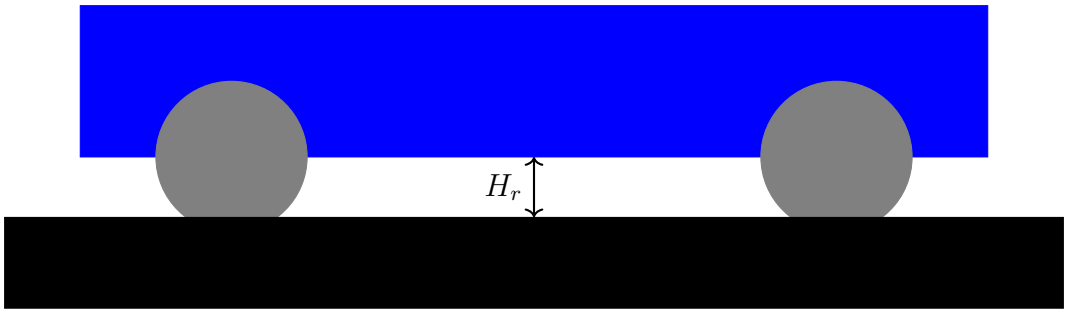

Figure 2.6: A ride height H_r.

2.3.6 Aerodynamic Influence on Vehicle Dynamics

Vehicle dynamics is a large and complex subject. Mass distribution, tires, suspension setup and aerodynamics are examples of areas that greatly affect the dynamics of a car. Basic principles of aerodynamics influence, in particular on a Formula student car, is further discussed here.

The main aim of aerodynamics on a Formula Student car is to increase its negative lift force (downforce). Greater downforce makes it possible for the tires to produce larger forces (grip) while accelerating/braking (longitudinal forces) and cornering (lateral forces). The basic formula describing this relationship is $F_{\text{long/lat}} = F_z\mu$, where $F_{\text{long/lat}}$ is the longitudinal or latitudinal force, F_z the normal force which is increased with increased downforce and μ the friction coefficient. Consequently, the speed of the car can be increased in most driving scenarios or the same grip can be achieved with less tire slip, i.e smaller slip angle, when compared to a car with less downforce. This helps reducing heat production and therefore preserve tire life. Furthermore, smaller slip angles are easier to control for the driver. The car's stability in this case is improved compared to larger slip angles and aerodynamic parts tend to work more efficiently, improving the balance [3].

In most cases a weight and aerodynamic distribution close to 50/50 on the cars

rear and front axle is desired. A car with the center of gravity (COG) closer to the front axle usually generates more understeer. Conversly the aerodynamic center of pressure (COP or aero balance), the point at which the resultant downforce is located, closer to the front usually generates more oversteer. A car with a front biased COG can therefore be counter balanced by placing the COP forwards. However, it is favourable in some cases, in CFS's case for example, to design the aerodynamic package with a COP slightly rear biased. This can generate understeer, but understeer is considered more stable and easier to control when compared to oversteer [3].

Vehicle dynamics parameters described in previous sections are closely related to the aerodynamic package on a given car. While the generated downforce affect body slip, pitch and roll angles, these parameters in turn affect the aerodynamic efficiency. Pitch angles for example can have a large impact on vehicle balance. When braking and pitching forwards, the front wing's downforce is generally increased. Although, other factors such as already low static ride height or an extreme pitch angle might cause a decrease in downforce for the front wing. This also results in less air flow to the car's floor and diffuser, decreasing the middle and rear downforce. If the front wing downforce increases, the aerodynamic balance shifts forwards, decreasing the stability of the car. While this is considered unfavourable, increased grip on the front axle also results in improved braking capabilities. On the contrary, if the downforce on the front wing decreases the balance shifts rearwards and the opposite occurs. It is more difficult to describe the influence of steering and roll angles. These affect the aerodynamics in an asymmetric manner and can cause unpredictable behaviour of the car. The same is true for body slip angles, or yaw angles, where the air flow hits the car with an angle from the longitudinal axis [3].

A diffuser expands the airflow underneath the car's floor. This expansion forces the flow upstream to increase in speed in order to fill up the larger volume in the diffuser, decreasing the pressure upstream. In motorsport it has been observed that diffusers are particularly effective aero devices. The reason is that diffusers increase the vehicle's downforce under the whole floor. Downforce in this region is close to the center of the car and distributed over a large aera. This results in good balance contribution and makes the vehicle less sensitive to pitch or other phenomena that affect the balance. In order for a diffuser to work efficiently, the front wing needs to supply the floor and diffuser area with sufficient airflow. Optimally the airflow's velocity is large and laminar. Another option for increasing the airflow is by feeding the diffuser with air from the sides of the vehicle. This can however interfere with the low pressure diffuser region and increase the pressure, resulting in a decrease of downforce. A compromise between keeping the floor sealed and increasing the airflow is usually optimal. This airflow can also be used to induce vortices, as described in the next section [3].

2.4 Working Principles of a Race Car Diffuser

The main function of an undertray diffuser is to reduce the pressure upstream of the diffuser, which provides a greater amount of downforce. Additionally, the diffuser

provides a smooth transition where the airflow under the car joins the wake region.

Equation (2.1) and Equation (2.2), can be combined to relate pressure, flow velocity and the area swept by the flow (i.e. the space between the car and the ground):

$$\frac{1}{2}\Big(\frac{\dot{m}}{\rho A_{\text{flow}}}\Big)^2 + \frac{p}{\rho} = constant, \tag{2.15}$$

Where the parameters are as in the previously mentioned equations. It is clear that a decrease in flow area promotes a decrease in pressure. Given the boundary condition of ambient pressure at the end of the diffuser, one can see that the diffuser promotes a negative pressure upstream, providing downforce.

However, this simplified model describes the undertray diffuser as a closed tube, in which the flow is perfectly laminar. A more accurate model would account for the air introduced from the gap between the diffuser sidewalls and the road as well as energy lost to complex, turbulent flow.

2.4.1 Effect of Different Design Parameters of the Diffuser

The geometry of a simple race car diffuser can be described by a number of key design parameters. These all have their respective effects on the airflow, and interact in complex ways.

2.4.1.1 Differences in the Angles of the Diffuser

The maximum angle of the diffuser channel's upper boundary relative to the xy-plane is referred to as *the expansion angle of the diffuser*. This angle determines to a great extent how well the flow attaches. A typical value is around 15°. A substantially higher angle will result in separation of the flow from the inside of the diffuser, resulting in an increase in pressure [13].

2.4.1.2 Differences in Area Ratio

The area ratio of a diffuser is related to the angle of the diffuser and the length of the diffuser volume by simple geometry.

$$R_{\text{ar}} = \frac{H_r + L_d \cdot \sin(\theta)}{H_r} = \frac{A_{\text{flow}}^{\text{init}}}{A_{\text{flow}}^{\text{final}}}, \tag{2.16}$$

where R_{ar} denotes the area ratio, θ the angle of the diffuser, H_r the ride height, $A_{\text{flow}}^{\text{init}}$ the inlet area of the diffuser, $A_{\text{flow}}^{\text{final}}$ the rear outlet area of the diffuser, and L_d the length of the diffuser volume.

Combining this equation with Equation (2.15) makes it clear that lower pressures can be obtained with longer diffusers and larger diffuser angles. However, a practical limit is reached when the area ratio approaches 1:5. At this point, the high pressure ambient air starts to interfere with and spoil the airflow, decreasing downforce [13].

2.4.1.3 Implementation of Strakes

Vertical panels in the diffuser volume, with the purpose of directing the airflow are referred to as strakes. Strakes lower the characteristic length of the flow, keeping the latter laminar and lowering the pressure. Other effects can be promoted by directing the airflow in different ways [3].

2.4.1.4 Different Throats of the Diffuser

The *throat* or *kick* of the diffuser is where the underfloor transitions to the diffuser ramp surface. The lowest pressure in the airstream is located in the throat, meaning that this area provides a non-negligible amount of downforce. The radius of this throat determines to some extent how the flow behaves inside the diffuser. A small radius will make the flow prone to separation downstream of the throat, but may also increase downforce by increasing underbody area [8].

2.4.2 Venturi Vortices

The performance of the diffuser is highly dependent on that the flow remains attached to the internal surface of the diffuser. As discussed, this stands in contrast to the measures taken to decrease pressure in and upstream of the diffuser. To keep the flow from separating, a vortex pair can be induced. The flow in such vorticies have a short characteristic length, and stay laminar to a greater degree. Methods to induce the desired vortices include:

- Direction of airflow over a sharp edge, such as over the diffuser sidewall
- Implementation of turning vanes, i.e. small winglets upstream of the diffuser, which give the flow closest to the car surface sideways momentum
- Implementing strakes in the diffuser channel, which contain and keep the vortices undisturbed.

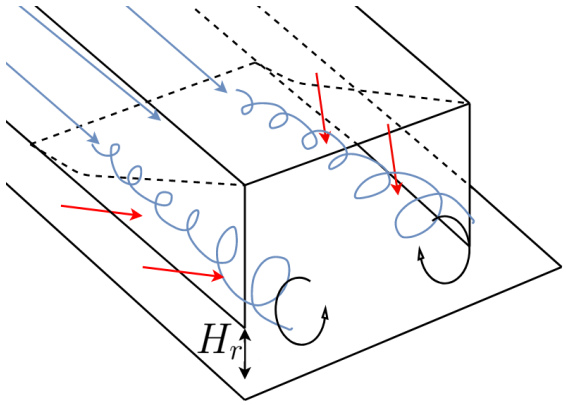

Figure 2.7: 3D-schematic showing the typical vortex pair that form as high-pressure ambient air flows into the low-pressure cavity of the undertray diffuser (red arrows). Note the direction of the vortex rotation. The blue streamlines are grossly simplified.

To some extent, the vortices also keep the high-pressure outside separated from the

low-pressure inside of the diffuser. This effect decreases pressure upstream of the diffuser, thus increasing aerodynamic performance [3].

3
Methods

The methods used in the project are presented in detail in this section. The workflow for creating and simulating a diffuser is shown in Figure 3.1.

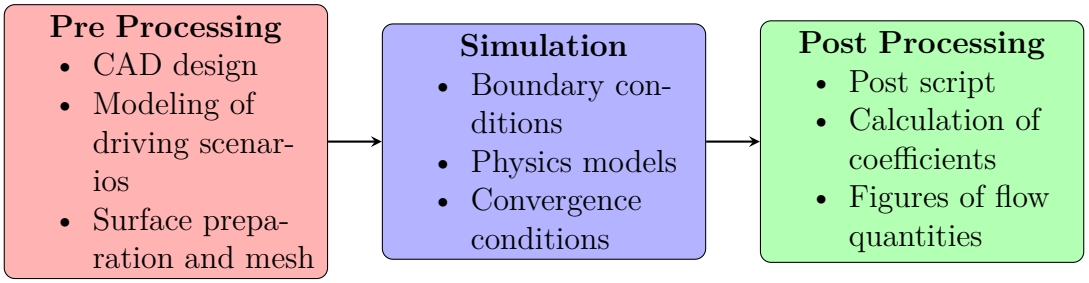

Figure 3.1: Workflow for the development of a diffuser.

3.1 CAD

To enable simulations of the Formula Student car a 3D-model was required. CAD was used to design all the geometries of the aerodynamics package before it was imported and pre-processed in the CFD software Star-CCM+. In order to create these CAD models, the software Catia V5 was used. The project was provided with the CAD model of the CFS21 car, i.e. the latest model, from which the design work could be based upon. The aerodynamic parts of the CFS car are shown in Figure 3.2. Since the project aims to study how a new diffuser could increase the performance of the formula car, all parts that were not connected to the diffuser could remain the same. Overall, only the diffuser and the monocoque were affected (in terms of direct contact) by the diffuser replacement. The monocoque is the self-supporting chassis of the car, which can be visualized in grey in Figure 3.2.

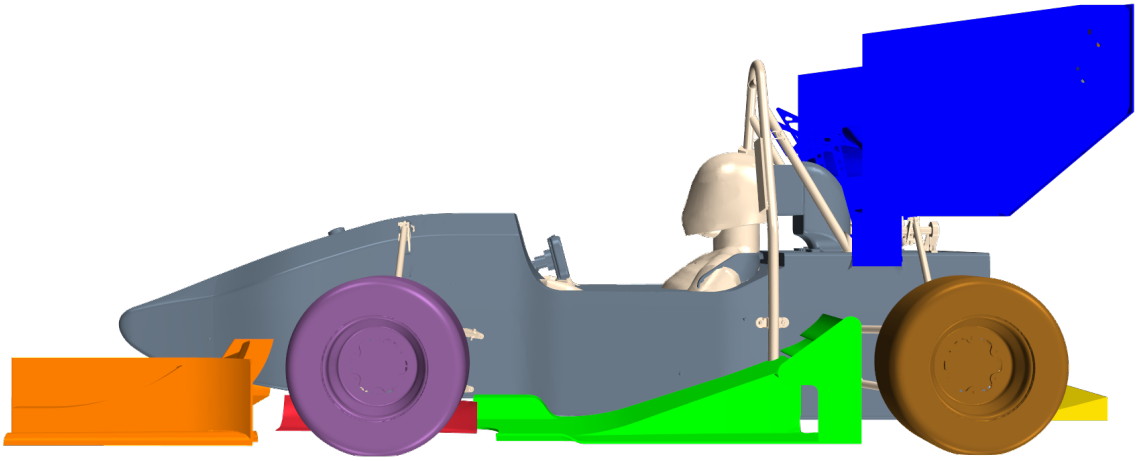

Figure 3.2: CAD model with the aerodynamic parts marked in different colors. Front wing (orange), deflector (red), monocoque (grey), side wing (green), rear wing (blue) and diffuser (yellow).

3.1.1 Current diffuser

As a starting point, a simplified version of CFS's latest diffuser was used. However, the current diffuser features an aggressive diffuser expansion angle which makes it difficult for the flow to remain attached. CFS21 has solved this by integrating the cooling package on the diffuser, and thus creating a suction normal to the flow direction. This results in a higher extraction of air and thus a higher downforce. The CFS21 diffuser is shown in Figure 1.1.

3.1.2 Design Methodology

To create a aerodynamically robust and well performing diffuser a number of design iterations were made.

The design methodology was based on a number of basic concepts. The concepts includes the effect of how early on the monocoque the diffuser can start as well as the the expansion angle of the diffuser. After these concepts had been tested and evaluated, more detailed components were added. These components were strakes and side floors.

As previously mentioned, the basic ideas of CFS's current diffuser were used as a starting point in the design development. Therefore, the first diffuser simulated had the same monocoque as CFS21. In order to start the design iterations with a basic geometry both side floors and strakes were not included. For the remaining design iterations it was chosen to redesign the monocoque. In that way, the diffuser could start earlier on the underside of the car, thus making the expansion of air more prolonged. It is considered an interesting aspect to study in order to find out if the downforce would increase.

The starting point of the diffuser, i.e how far from the back of the monocoque the diffuser starts, was iterated. The two extreme cases of starting the diffuser as early as possible (500 mm in front of the monocoque rear wall) and as late as possible (coinciding with the monocoque rear wall) were tested. An alternative concept between the extreme cases was also tested, where the diffuser instead started 300 mm in to the monocoque. All three designs are displayed in Figure 3.3. The 300 mm design was similar to the 500 mm case. Their difference being that the 300 mm starting point resulted in a smaller throat radius connecting the flat underfloor and the diffuser's final angle of 15°. It was then possible to draw conclusions regarding which design showed the most potential and attachment of flow.

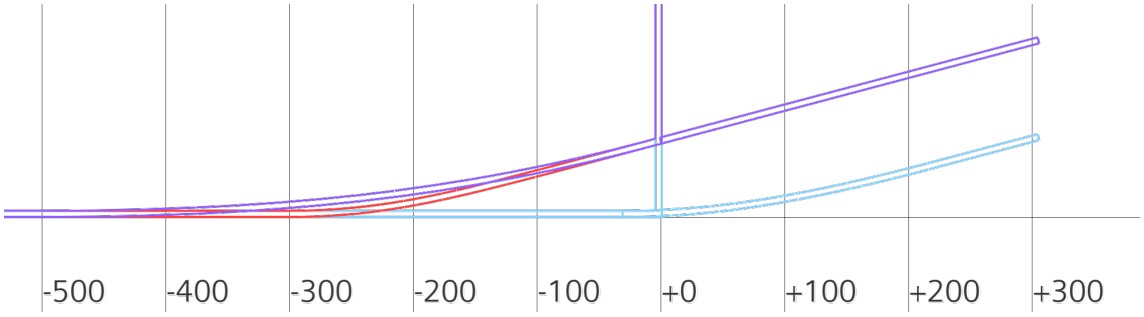

Figure 3.3: Outlines of the three different diffuser designs when iterating the starting point of the diffuser. The 500 mm design is displayed as purple, the 300 mm design as red and the 0 mm design as blue.

The angle between the flat bottom of the monocoque and the top of the diffuser was also iterated. The angles tested were 13°, 15°, 17° and 19° which are displayed in Figure 3.4. The project group chose to test four different angles due to time limitations, especially in terms of simulation time. 15° was estimated to be the angle corresponding to a reasonable movement of electronics in the rear of the current CFS car. The other three angles were chosen at a linear scale to see how both slightly higher and lower angles affect the diffuser.

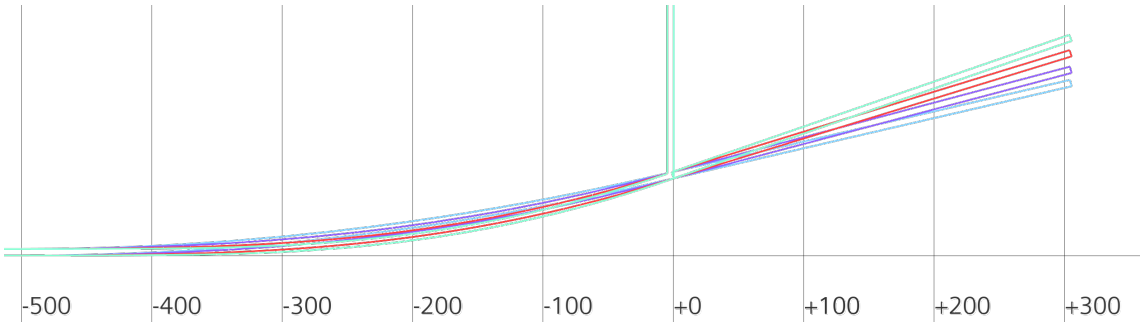

Figure 3.4: Outlines of the four different diffuser designs when iterating the angle between the flat bottom of the monocoque and the top of the diffuser. The 13° design i displayed as blue, the 15° design as purple, the 17° design as red and the 19° design as green.

After these basic design concepts had been tested, strakes and side floors were added to the designs that had performed best so far. The idea behind adding strakes was to induce more vortices and the idea behind side floors was to enlarge the low pressure surface of the diffuser, both adding downforce. Strakes were added by copying the outer walls of the diffuser and placing the copies at a fourth of the diffuser's width symmetrically around the middle line. The side floors were designed with the same width as the current CFS car's side floors. See Figure 3.5 for details.

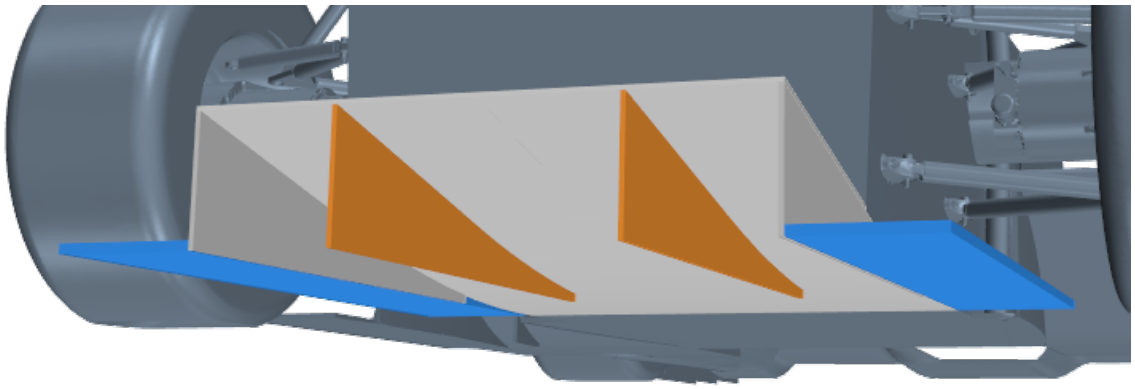

Figure 3.5: Diffuser with both strakes (orange) and side floor (blue).

3.2 CFD

As computer performance has increased over the recent decades, computational fluid dynamics have become a more powerful tool. This section contains the setup for the simulations.

3.2.1 Whole-car Versus Half-car Symmetry Simulation

Previous CFS teams have mostly used a half-car symmetry model for the simulations in the design process. The near-symmetric geometry of a car was exploited to decrease the computational resources needed. This resulted in less computing time and more simulations. However, due to the asymmetric flow during cornering, a half-car symmetry simulation is not possible for all scenarios. Previous CFS teams have also noted discrepancies between the two simulation models' results. This might be due to small asymmetries between the car's left and right features and geometry. Another cause might be that the symmetry plane boundary conditions of the half-car symmetry simulation are over-simplified. To ensure comparable results for the different simulated scenarios, it was decided to only do whole-car simulations. This trade-off increases simulation run time, but provides greater confidence in the simulation results.

3.2.2 Physics Model

All the physics models were taken from CFS's previous simulations, and can be seen i Table 3.1. Star-CCM+ is set to use SST $k - \omega$ turbulence modeling because it

uses the advantages of both $k-\omega$ turbulence modeling near the walls, and $k-\epsilon$ modeling in the far-field. The properties of each turbulence model are discussed in Sections 2.2.2 to 2.2.4.

Table 3.1: The settings used in Star-CCM+.

Settings
All y^+ Wall Treatment
Cell Quality Remediation
Constant Density
Exact Wall Distance
Gas: Air
Gradients
$k-\omega$ Turbulence
Reynolds-Averaged Navier-Stokes
Segregated Flow
Solution Interpolation
SST (Menter) $k-\omega$
Steady
Three Dimensional
Turbulent
Wall Distance

3.2.3 Mesh

The meshing procedure in Star-CCM+ is done with three operations. First a surface wrapper is executed over the car. Subsequently, the wrapper is subtracted from the wind tunnel. Lastly an automated mesh is run on the subtract.

3.2.3.1 Surface Wrapper

A surface wrapper with a base and gap closure size of 32 mm and 5 mm respectively were applied on the car's surface. The target surface size was 16 mm and the minimum surface size 2 mm. Contact prevention groups were created for the geometry so parts did not "smudge" together. Contact prevention were done on the front wing, rear wing, monocoque, roll hoop, side diffusers and rear diffuser.

3.2.3.2 Volume Mesh

The base size of the volume mesh was 32 mm, the target surface size 16 mm and the minimum surface size 2 mm. Trimmed cells were used so that cell size could be increased far from the car to lower the cell count. The mesh is illustrated in Figure 3.6. Where gradients in for example pressure and velocity were large, a finer mesh was created with volumetric controls. The volumetric controls were mainly inherited from CFS. The prism layer settings were inherited from CFS and consisted of 12 layers and an increase between layers of 1.2 with the all the layers' thickness being

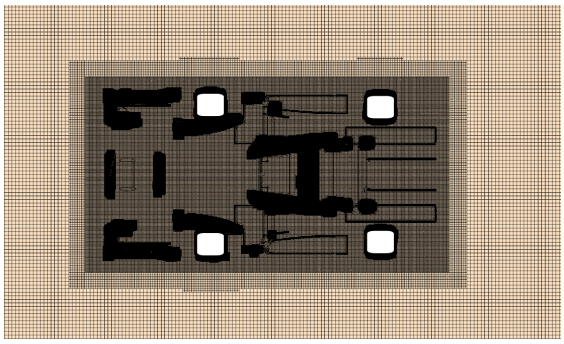

(a) Mesh in xy-plane located $z = 5$ cm above ground

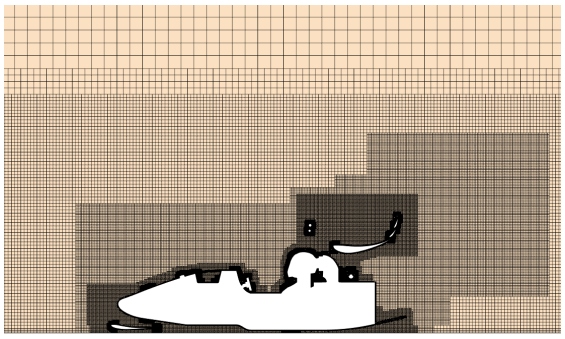

(b) Mesh in xz-plane through the middle of the car

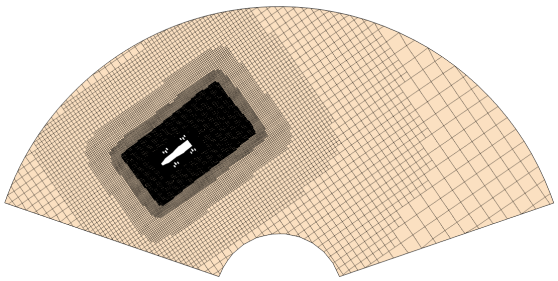

(c) Mesh in xy-plane located $z = 25$ cm above ground for cornering.

Figure 3.6: Volume mesh for the simulations.

10 mm. This gave good y^+-values (see Section 2.1.6.2) that were below 5 for the inner prism layer as can be seen i Figure 3.7. The total amount of cells were around 52 million for the straight case and 53 million for the curved case.

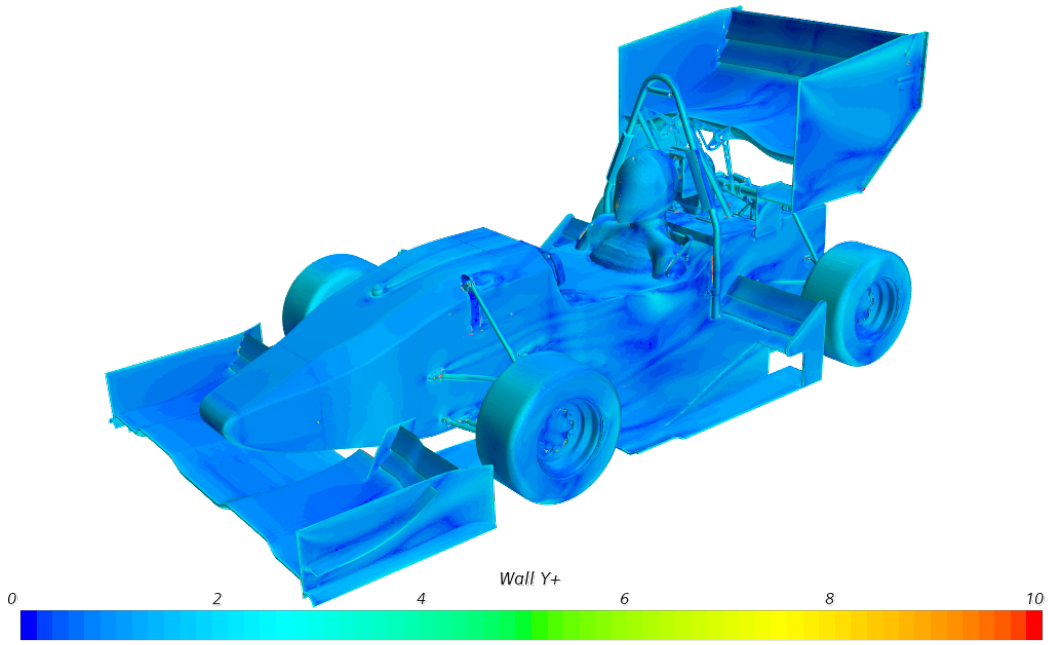

Figure 3.7: The Wall y+ for the inner prism layer around the car.

3.2.4 Boundaries

The boundary conditions differ slightly depending on if a straight or a cornering simulation is too be performed. The boundaries for the case when that car is driving straight can be seen in Table 3.2.

Table 3.2: The boundaries for a straight simulation.

Boundary	Boundary Condition	Value
Wind tunnel inlet	Velocity inlet	[40, 0, 0] km/h
Wind tunnel outlet	Pressure outlet	0 Pa
Wind tunnel roof, walls	Symmetry plane	-
Wind tunnel ground	Moving wall	[40, 0, 0] km/h
Wheels	Rotating wall	48.6 rad/s around wheel axis
Car except wheels	Wall	0 km/h

The boundaries for the case when the car is cornering can be seen in Table 3.3. As can be seen, the velocity of the inlet and ground is 0, that is because parts of the system is in a rotating reference frame [14]. This reference frame contains the fluid volume and outer boundaries which rotates at 0.889 rad/s. This comes from dividing the speed of the car's center of gravity, 40 km/h, with the corner radius 12.5 m. The car on the other hand is fixed at the same point with only the wheels spinning around their own axis.

Table 3.3: The boundaries for a cornering simulation. For an accurate representation the system has to be viewed in a rotating reference frame. The reference frame contains the fluid volume and outer boundaries which rotates while the car is fixed.

Boundary	Boundary Condition	Value
Wind tunnel inlet	Velocity inlet	[0, 0, 0] km/h
Wind tunnel outlet	Pressure outlet	0 Pa
Wind tunnel roof, walls	Symmetry plane	-
Wind tunnel ground	Moving wall	[0, 0, 0] km/h
Wheels	Rotating wall	48.6 rad/s around wheel axis
Car except wheels	Wall	0 km/h

3.2.5 Simulation

The initial condition for the velocity of the air was set to [40, 0, 0] km/h. Because of the turbulent nature of this simulation, the residuals will never fully converge so the simulation is run for 3000 iterations. The mean values for coefficients from the last 500 iterations are saved. This is because the simulation's fields always has some fluctuations.

3.2.6 Post Processing

The post processing consisted mainly of two types of analyses: numeric values and visualized flow fields. The numeric values were obtained by using the built in features, monitors and reports, in Star-CCM+. A report had to be set up for each variable of interest. The monitor would then store values generated by a report, one set of values for every iteration of the simulation. These values was then be averaged over the last 500 iterations to get a representative value. The visualized flow fields were obtained by visualizing the solution of one variable on either the surface of the car or on a cross section plane of the simulated volume. These flow fields were not averaged but instead only contained data from the last iteration of each simulation.

For the cornering scenario a field function and sum report was used to calculate some of the force and force coefficients. This was required since the surrounding air flow was curved and the direction of the force had to be calculated in the direction of the flow. The field function was therefore defined so that at every cell the force or force coefficient was computed in the same direction as the curved flow in the specific cell [15]. These values could then be summed up to get the total value of interest. This methodology was used to get the correct values and representations for the drag coefficient, the total pressure coefficient and the skin friction coefficient.

3.3 Choice of Simulated Driving Scenarios

Historically, CFS has only simulated a neutral-attitude half-car driving straight ahead during the design process. Although some simulations of different driving

scenarios have been done, these have not been taken into consideration in the design process as they were in this project.

The most accurate data on aerodynamic sensitivity would be acquired by simulating as many scenarios as possible. However there is a practical limitation from the computational resources available for the simulations. Hence a small number of common and critical maneuvers need to be identified and implemented into the simulations. Each whole-car simulation takes about 4 hours to run on the computational cluster provided by Swedish National Infrastructure for Computing (SNIC). This corresponds to approximately 600 core-hours. Given the available resources for both this project of 10 000 core-hours/month and for future CFS teams of 20 000 core-hours/month, the optimum number of simulated scenarios for each design was assessed to be three.

The aim of each simulation is to acquire data that describe the real-world performance of the vehicle. There is a number of different driving scenarios where aerodynamic downforce is critical. The most demanding maneuvers (driving scenarios) with the highest lateral and longitudinal accelerations, i.e. where downforce is the most needed, are braking and cornering [3]. This is supported by raw data collected by CFS during the 2016 Formula Student Germany Endurance competition. The data also suggests that the largest portion of the lap time is spent cornering, making this maneuver the most important for improved lap times. Furthermore, Figure 3.8 illustrates that the forces during braking are larger compared to accelerating forwards. This implies that downforce is more important during braking. Due to the mentioned resource and time restrictions within this project, the forwards-acceleration scenario was excluded. Only cornering and braking were simulated along with straight driving with a neutral attitude, the latter for reasons mentioned below.

The magnitudes of certain parameters to implement, such as speed, corner radius and steering angles are based on simulations and real world data from previous CFS teams. In addition, the current CFS21 team has been involved in discussions and has been offering guidance.

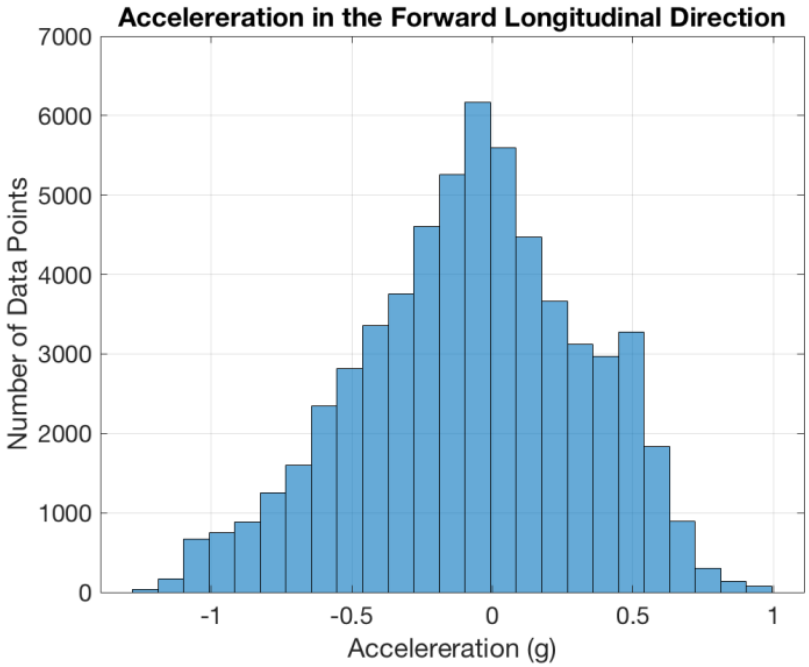

Figure 3.8: GPS data from a lap of the 2016 Formula Student Germany Endurance circuit from the CFS16 car. A histogram of longitudinal acceleration in the forward direction is illustrated.

3.3.1 Assertion of Reynolds-independence

Simulation data from previous evaluation of the CFS20 car was provided for analysis. The data was analyzed as to establish that the flow is largely Re-independent, i.e. that the aerodynamic forces increase with the square of u_∞. The data were fitted in MATLAB to a function of the following form:

$$F_{\text{aero}} = a \cdot u_\infty^2, \tag{3.1}$$

where a is an arbitrary constant. Data for $40, 60, 80, 100$ and 120 km/h were available. For all forces on separate aerodynamic components, the minimum coefficient of determination (R^2) of the fit was 0.996. This was regarded to be a very good fit, proving that simulations with a single value of u_∞ also are representative for different values in the relevant span.

3.3.2 Driving Straight Ahead

Although downforce is of the least relevance when driving straight ahead at neutral attitude, as the car doesn't accelerate in any direction, it was decided to include it in the list of scenarios. This decision was made to provide a basic understanding of the characteristics of each diffuser design. Additionally, this made comparisons with simulation data from previous diffuser designs possible. The ride height was set to 30 mm as recommended by the current CFS21 team. Contribution from aerodynamic load on the ride height has been shown to negligible and is therefore

neglected. The car's velocity was chosen as 40 km/h to be comparable to previous CFS aerodynamic simulations and is further discussed below.

3.3.3 Cornering Driving Scenario

To simulate cornering as realistically as possible, real world GPS data was used to determine the most frequent corner radius and vehicle speed. The data used was acquired by CFS16 during the endurance race of the Formula Student Germany competition in 2016 and is presented in Figure 3.9. The most frequent corner radius was determined to be 12.5 m and corresponding speed 40 km/h.

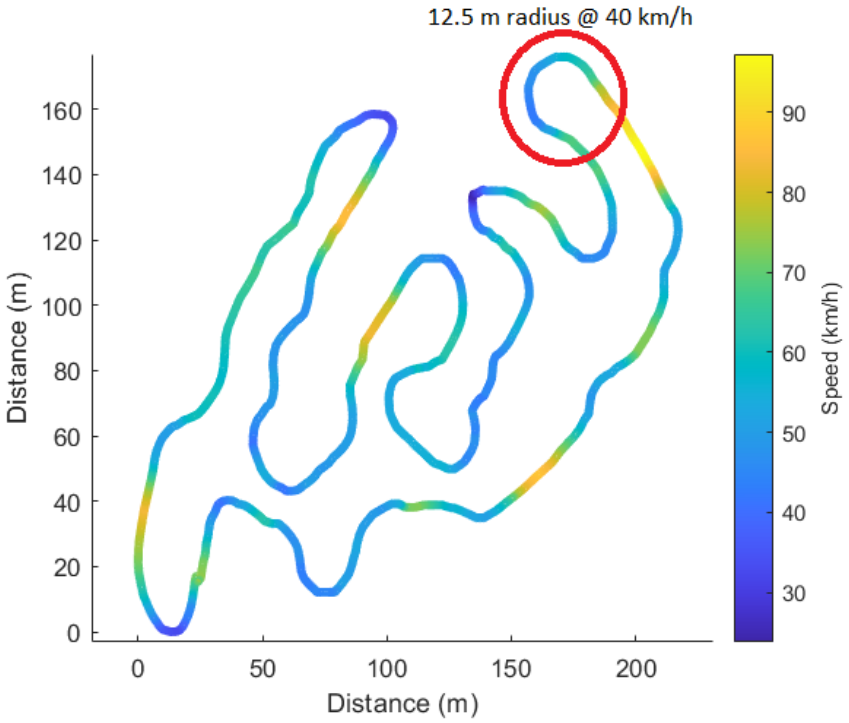

Figure 3.9: GPS data from a lap of the 2016 Formula Student Germany Endurance circuit from the CFS16 car. A typical 12.5 m radius corner where the average recorded speed is approximately 40 km/h is marked in the figure.

While cornering the vehicle dynamics differ from when driving straight. Steering angles for the front wheels, body slip and a roll angle need to be accounted for. These angles are discussed in Section 2.3. The quantities of these angles can be found in table 3.4, note that the angles are given for a corner with radius 12.5 m and a speed of 40 km/h. The steering and body slip angles used were the same as the ones used in CFS20 and are based on simulations. The roll angle was acquired from the suspension group of the CFS21 team as $0.7°/g$, where g is the lateral acceleration and $1g \approx 9.81$ m/s^2. For a 12.5 m radius corner and vehicle speed of 40 km/h this equates to almost exactly 0.7°. Vehicle pitch was not considered as the scenario simulated does not include longitudinal acceleration. Furthermore, only left hand corners were simulated as CFS20 cornering results showed no significant difference between left and right cornering.

Table 3.4: Angles for simulating cornering at a corner radius of 12.5 m. For details regarding the different parameters, see Section 2.3.

Angle	Value
Inner steering angle	7.18°
Outer steering angle	7.36°
Body slip angle	3.5°
Roll angle	0.7°

3.3.4 Braking Driving Scenario

While braking, the vehicle rotates with a pitch angle around an axis called the pitch center. The pitch angle for hard braking can be approximated to when the front wing almost scrapes the ground which is approximately 1.0°. This is based on observations from the CFS team. Although such steep angles are only achieved while braking from speeds exceeding 60 km/h, a speed of 40 km/h was chosen for this scenario. The flow has been shown to be Reynolds number-independent as previously described and the chosen speed of 40 km/h will therefore not influence the normalized results. This means that the resulting fields behave the same as they would at 60 km/h. The resulting forces can be multiplied by a factor of $\left(\frac{60}{40}\right)^2$ to yield the same results as a simulation at 60 km/h, since the forces scale with a factor of u^2. Furthermore, the braking scenario is directly comparable to the straight and cornering scenarios if they are all simulated at the same speed, in this case 40 km/h, and the scaling of data and plots is then identical.

4
Results and Analysis

In this chapter the results of this study are presented and analyzed. The objective of the study was to identify which driving scenarios to simulate, as well as investigate the car's aerodynamic performance during these maneuvers with several different diffuser designs. This chapter will discuss both of these issues.

Much attention will be dedicated to analysis of the flow patterns and their generation of downforce. Due to the small number of data points, no extrapolation nor interpolation is done from the parameter sweeps. Instead, a more discussion-based presentation of results is favored. The main focus is on downforce generation as described in Section 1.4.

Firstly, a general comparison of the three driving scenarios straight, braking and cornering is made. Design iterations are later compared where, to minimize the number of figures, only the most relevant results are presented.

4.1 General Differences for Driving Scenarios

In this section general observations and results for the three driving scenarios: straight, braking and cornering are compared. The smallest diffuser design, with a starting point coinciding (0 mm) with the back of original flat-bottomed monocoque used in CFS20 and CFS21 (see Figure 3.3), is used as a baseline for this comparison. Although a specific design is used, most of the observations made apply to every design iteration in this project.

Table 4.1: Values for C_D, C_L for different components and aero balance (rearwards) for different driving scenarios using the small diffuser starting at the end of the monocoque. M&D stands for Monocoque & Diffuser, FW for Front Wing, RW for Rear Wing and SW for Side Wing.

Scenario	C_D	C_L	C_L M&D	C_L FW	C_L RW	C_L SW	Aero balance
Straight	1.433	3.612	0.435	1.352	1.032	0.862	50.06%
Cornering	1.302	3.544	0.436	1.325	0.983	0.882	49.90%
Braking	1.355	2.799	0.336	0.773	1.013	0.733	67.17%

The largest simulated downforce is obtained in the straight driving scenario, with cornering not far below, as can be seen in table 4.1. The losses come from the front

wing, where C_L decreases from 1.352 to 1.325 (2 %) and the rear wing's C_L decrease from 1.032 to 0.983 (5 %). With such small changes, the aero balance is very similar for the two cases. It is important to note that not only C_L M&D is affected by the different driving scenarios, but other aerodynamic components as well. The same is true when comparing different diffuser designs as seen later in Table 4.3. In the current example, the diffuser gains downforce while the car and the other aero components are losing, resulting in a worse overall package. Therefore, total downforce is the most relevant metric to analyze.

When the car pitches during braking the downforce loss and consequently aero balance change is significantly greater. The largest contributor is the front wing which loses 0.580 C_L, from 1.352 to 0.773 (43 %). As a result, the aero balance is greatly shifted rearwards. Furthermore, the side wing C_L decreases from 0.862 to 0.733 (15 %) and M&D C_L drops from 0.435 to 0.336 (22 %). The drag force coefficient C_D follows the same pattern as C_L and proves that larger downforce tends to result in increased drag force.

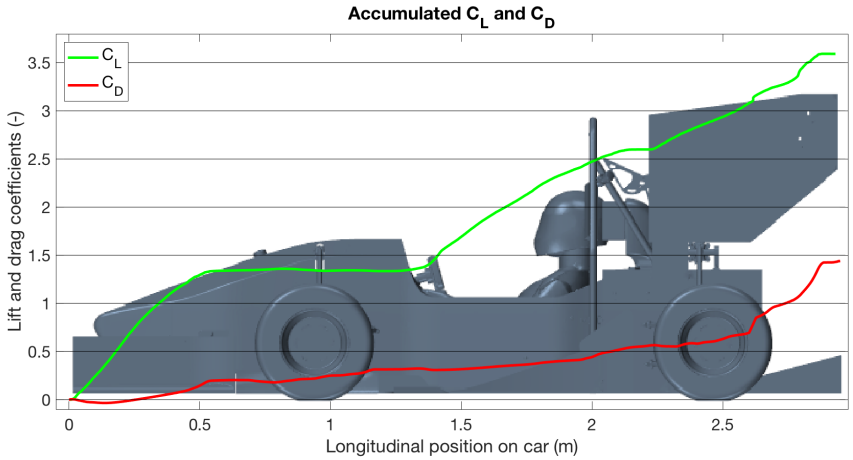

Figure 4.1: Accumulated C_L and C_D while driving straight for the whole car with the small diffuser attached to the original CFS20 and CFS21 monocoque.

The downforce C_L and drag C_D distribution of the car while driving straight is presented in Figure 4.1 as accumulated plots. It is clear that the downforce distribution is not uniform. Instead distinct inclinations can be seen around the front wing at $x = 0 - 0.5$ m, the side wings & underfloor at $x = 1.3 - 2.2$ m and the rear wing & diffuser at $x = 2.2 - 3$ m. On the contrary, the drag force distribution is more uniformly distributed with the only large increases right behind the monocoque at $x = 2.6$ m and the rear wing flaps at $x = 2.8$ m. This is due to the large wake created as seen in Figure 4.3.

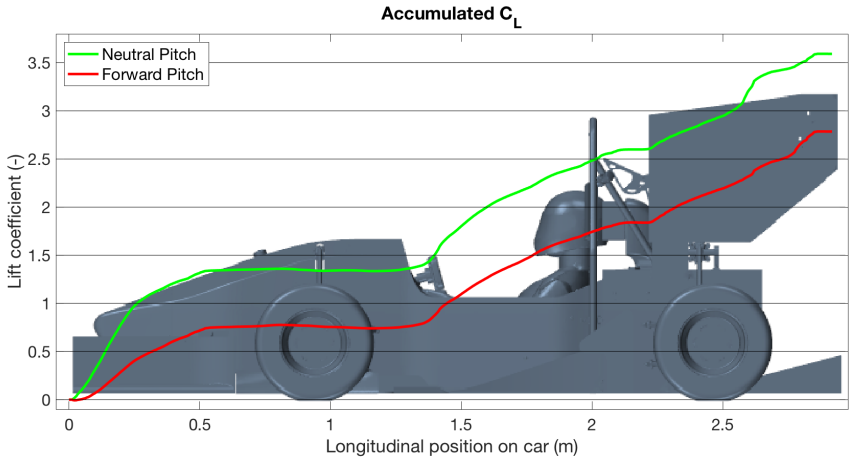

Figure 4.2: Accumulated C_L for the braking scenario compared to the straight scenario for a diffuser starting after the monocoque.

The straight and braking scenarios are compared above in Figure 4.2 where their respective accumulated lift coefficients C_L are presented. The performance of the front wing is severely impaired by the limited air flow under the front wing. The fact that the lines are approximately parallel downstream of the front wing suggests that the other parts of the aerodynamic package remain largely unaffected by the difference in pitch angle. However, another distinction is seen after the step in the underfloor, located around $x = 1.5$. The generated downforce is further decreased after this section, again suggesting that the air flow is reduced. Small pressure differences in the diffuser are not visible here, but are noted in Figure 4.5.

4.1.1 Differences in Velocity Magnitude

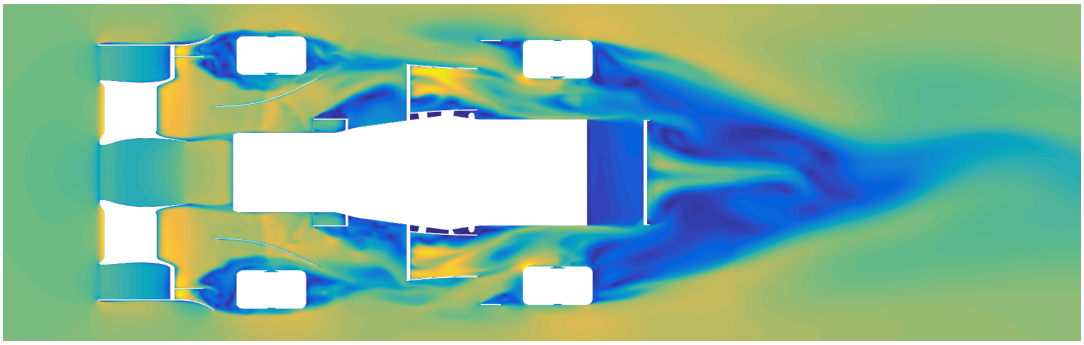

(a) Straight driving scenario.

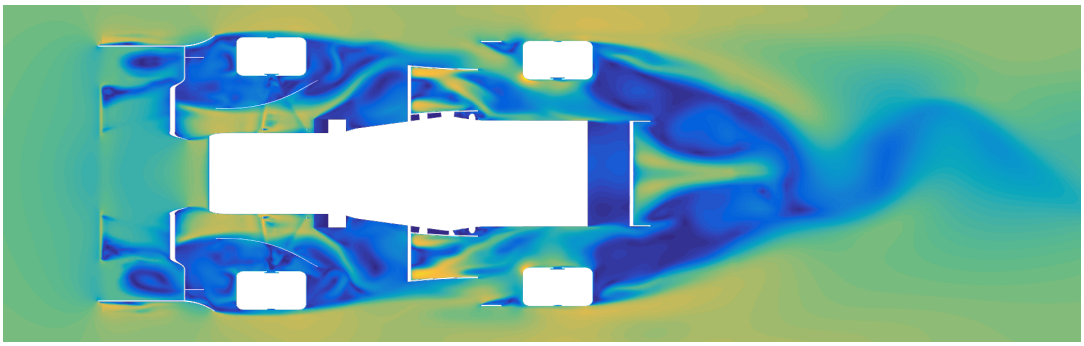

(b) Braking scenario.

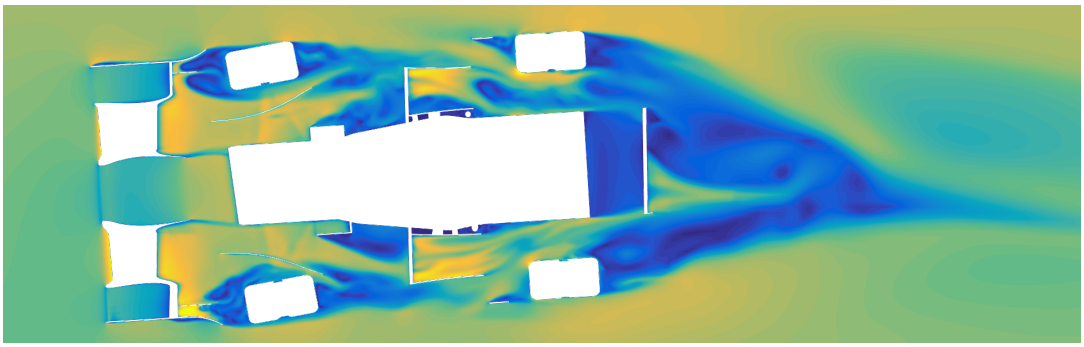

(c) Cornering scenario.

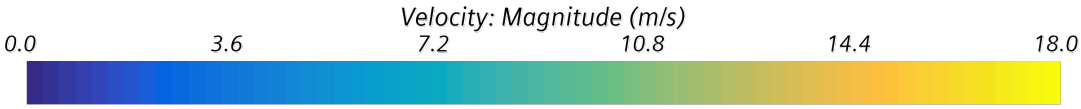

Figure 4.3: Velocity magnitude plots for driving straight, braking and cornering with the small 0 mm starting point baseline diffuser. The visualised xy-plane is located at $z = 88$ mm above ground.

The air flow velocity magnitude of the three simulated driving scenarios is presented in Figure 4.3. The air flow velocity determines how much downforce is generated. This velocity is decreased between the front wheels while braking with a pitch angle, see Figure 4.3b, compared to driving straight, see Figure 4.3a. This explains the heavily reduced downforce while braking. The lowered front wing is the cause since the area beneath it is smaller, reducing the air flow. For further visual comparison,

see Figure 4.4. Lower velocity in this area affects the other aerodynamic components further downstream, reducing the available air flow to produce downforce. However, the rear wing, which is located higher than every other aerodynamic device, is comparably unaffected and only lost 1-2 % of its downforce. It is unclear why this loss occurs since the high velocity region beneath the wing is larger during braking in Figure 4.4, implying lower pressure as described by Bernoulli's principle in Section 2.1.1. One explanation could be that the rear wing's angle of attack is increased past the optimum, resulting in slight detachment of the flow.

The air flow while cornering differs in many ways. Although the results only point to a small decrease in downforce, the air flow behaves differently. Combined consequences of the curved air flow and body slip makes the air interact with the car at different yaw angles. As a result, the velocity field is asymmetric. Figure 4.3c shows that the high velocity air is pushed to the left (bottom in the figure) diffuser wall, inducing a strong vortex in this region.

(a) Straight driving scenario.

(b) Braking scenario.

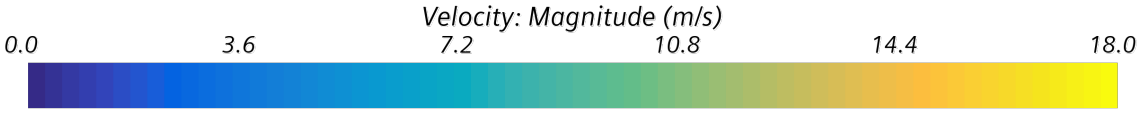

Figure 4.4: Velocity magnitude plots for the air surrounding the car. The visualized xz-plane is located in the middle of the car at $y = 0$. Only the straight and braking scenarios are included.

Only the straight and braking scenarios are shown in Figure 4.4. Visualizing the curved air flow during cornering in a flat plane would not provide any useful observations. The previously mentioned reduction of flow beneath the front wing is once again apparent. In addition, it seems that separation occurs as indicated by the blue low velocity area. Lower velocity and more separation tends to result in lower downforce since the pressure difference between the top and bottom of the wing is reduced. Furthermore, the air flow velocity of the side wings and diffuser is decreased. The resulting pressure differences which lead to the downforce losses are presented in the next section.

4.1.2 Differences in Pressure Coefficient

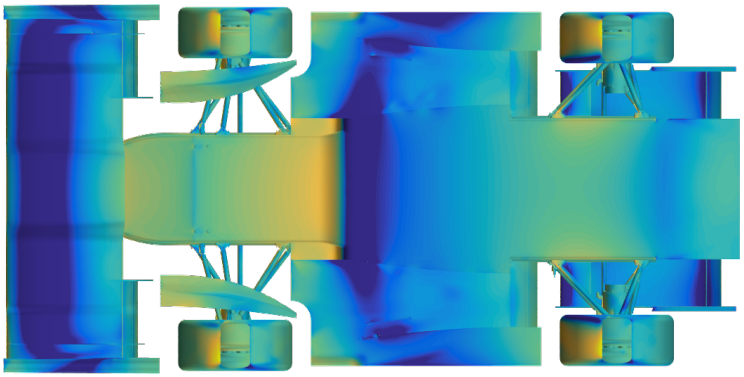

(a) Straight driving scenario.

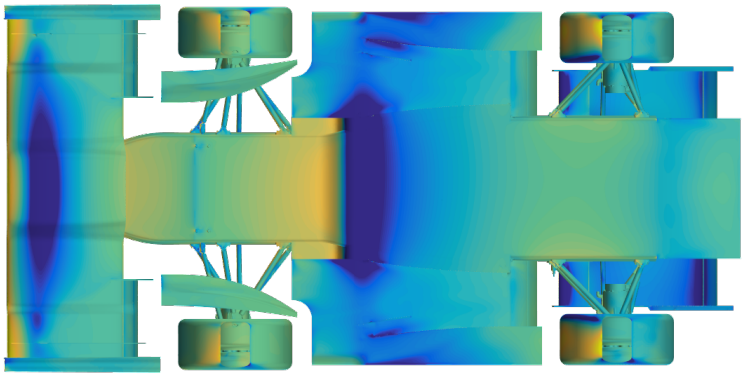

(b) Braking scenario.

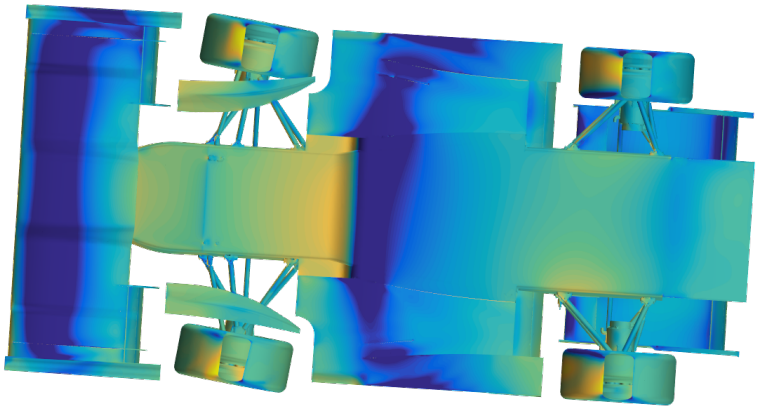

(c) Cornering scenario.

Figure 4.5: Pressure coefficient on the underside surface of the car during the three driving scenarios straight, braking and cornering.

The pressure coefficient on the car's underside can be seen in Figure 4.5. In all scenarios there is a low pressure region under the front wing, under the side wings, behind the step in the underfloor of the monocoque and where the diffuser starts. The difference is that in the cornering scenario (Figure 4.5c), the low pressure area is bigger on the left hand side (the top of the figure) than the right hand side (the bottom of the figure). This means that the downforce is larger on the inside half of the car while cornering. The braking scenario (Figure 4.5b) has an area of high pressure at the start of the front wing and a smaller low pressure area. This is a consequence of the front wing separation and reduced air flow as mentioned in the last section. Furthermore, the low pressure region behind the monocoque step in the underfloor is narrower when compared to the straight scenario. The same is true for the low pressure area at the start of the diffuser and the side wings, further indicating that the air flow and downforce is restricted.

(a) Straight driving scenario.

(b) Braking scenario.

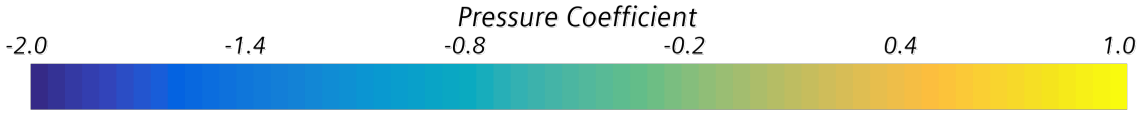

Figure 4.6: Pressure coefficient of the air surrounding the car. The visualized xz-plane is located in the middle of the car at $y = 0$. Only the straight and braking scenarios are included.

In Figure 4.6 the pressure coefficient can be seen in a plane through the middle of the car ($y = 0$) for the straight scenario (Figure 4.6a) and the braking scenario (Figure

4.6b). As previously mentioned, cornering is excluded since a straight plane would not produce any useful information from a curved air flow. It is noticeable when comparing the two scenarios that the braking scenario shows a smaller low pressure region under the front wing. This is again due to the reduced air flow resulting from the pitch angle. In addition, the low pressure area in the throat of the diffuser is smaller. The overall higher pressure underneath the car is generating less downforce compared to the straight scenario.

4.1.3 Differences in Skin Friction Coefficient

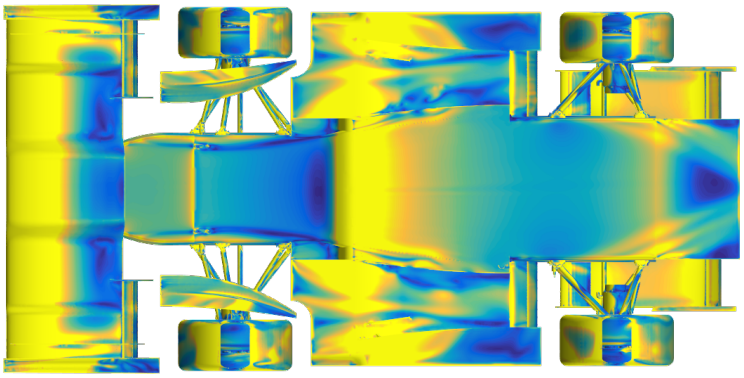

(a) Straight driving scenario.

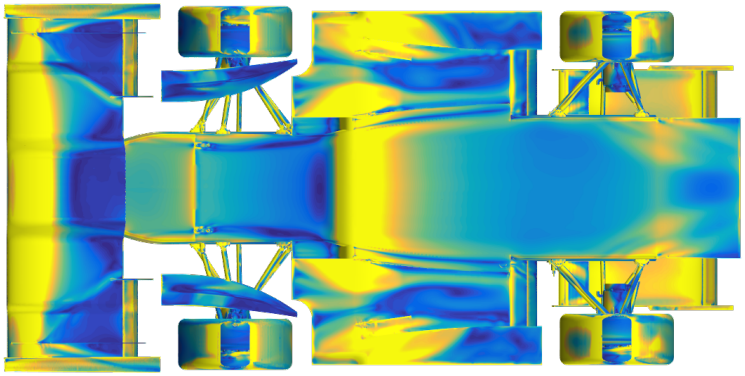

(b) Braking scenario.

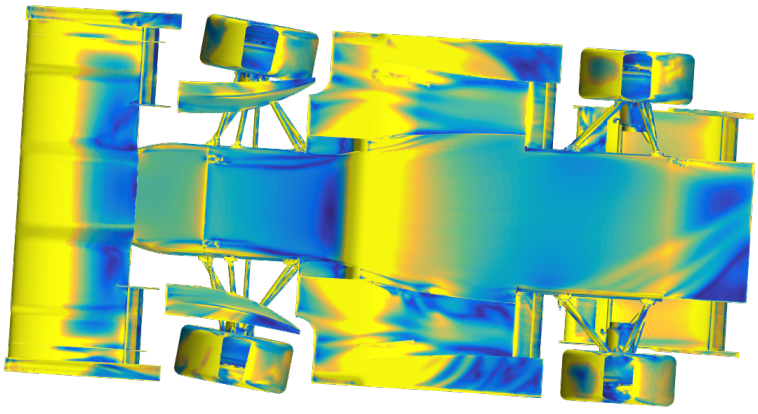

(c) Cornering scenario.

Figure 4.7: Skin friction coefficient on the car surface seen from below.

The skin friction coefficient C_f on the surface of the car for the different driving scenarios can be seen in Figure 4.7. Skin friction correlates to attachment and sepa-

ration. Greater skin friction (yellow in Figure 4.7) corresponds to more attached and energetic flow, whereas smaller skin friction values (blue in the figures) corresponds to more separated flow. A separation bubble is seen in the middle of the diffuser in the straight scenario in Figure 4.7a and the braking scenario in Figure 4.7b. If this separation bubble grows too large, stalling may occur resulting in sudden loss of downforce. The bubble seems larger in the straight compared to the braking scenario. The cornering scenario in Figure 4.7c seems more similar to the straight in this regard, but the separation bubble is twisted, following the curved air flow.

The yellow lines in the diffusers are in the next section shown to be vortices. Vortices contributes with improved flow attachment, driving the air to the ceiling of the diffuser, minimizing the separation bubble. Increased skin friction coefficient corresponds to stronger vortices in this case.

Separation differences are clear on the front wing surface. As described in previous sections, considerable separation occurs during braking as seen in Figure 4.7b when compared to the straight scenario seen in Figure 4.7a. Furthermore, the high skin friction area at the step in the monocoque underfloor is reduced while braking, explained by the reduced air flow.

4.1.4 Differences in Vorticity Magnitude

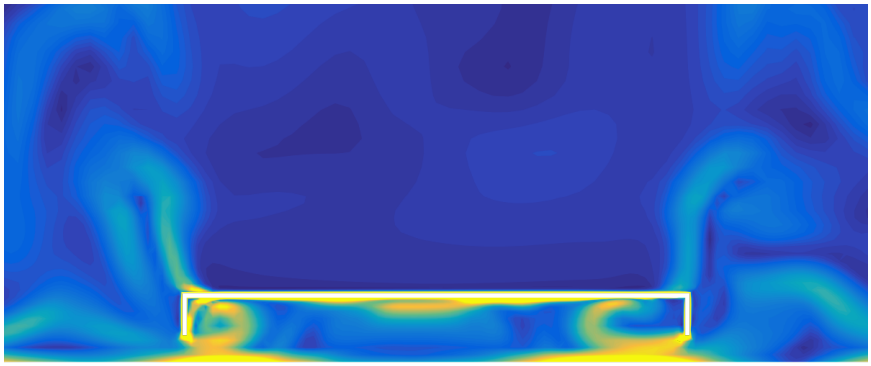

(a) Straight driving scenario.

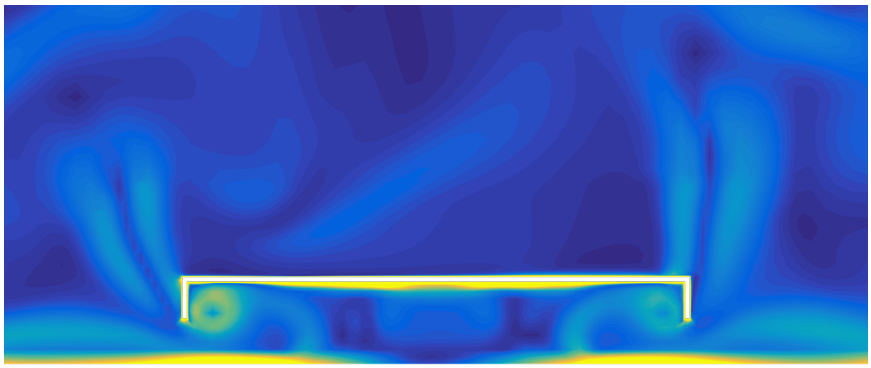

(b) Braking scenario.

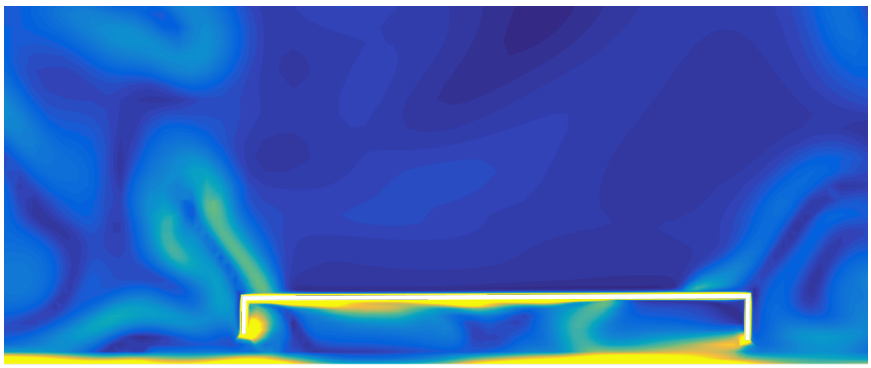

(c) Cornering scenario.

Figure 4.8: Vorticity magnitude for driving straight, braking and cornering. The visualized yz-plane is cutting through the diffuser 230 mm behind the monocoque.

The vorticity magnitude in the diffuser in the different scenarios can be seen in Figure 4.8. What can be seen from the straight scenario (Figure 4.8a) is that there is high vorticity near the diffuser walls. There is also some vorticity in the middle of the diffuser near the ceiling that originates from the turbulent separation bubble.

The vortices in the braking scenario (Figure 4.8b) are not as prevalent as in the straight scenario because of the reduced air flow to the diffuser. As described previously, this corresponds to a lower skin friction coefficient. In the case of cornering, it can be seen that the vortices are more asymmetric compared to when driving straight and braking. As can be seen in Figure 4.8c, a stronger vortex is generated in the left edge of the diffuser wall. This is expected since the car is simulated turning left and is correlated to the larger skin friction coefficient on the left side of the car, seen in the previous section. The flow that passes through the diffuser from the front wing and underneath the car, as well as from the side of the car, does not occur symmetrically. This explains the asymmetric formation of vortices when cornering.

4.2 Starting Point of the Diffuser

First the start of the diffuser was investigated and the data from simulations when altering the starting point can be found in Table 4.2. The different designs, visualized in Figure 3.3, showed similar performance in regards to drag and lift coefficients. However a difference can be seen for the M&D contribution to the lift coefficient. The 300 mm design gave better M&D performance for the straight and braking scenarios while losing performance during cornering. The aero balance also shifts the most while braking for the 300 mm design. This suggests the design is less stable and therefore not giving the desired robustness.

Table 4.2: Values for C_D, C_L, C_L M&D and aero balance (rearwards) for the different diffuser starting points at the driving scenarios straight, cornering and braking.

Design	Scenario	C_D	C_L	C_L M&D	Aero balance
500 mm	Straight	1.424	3.639	0.483	50.36%
	Cornering	1.408	3.542	0.417	49.62%
	Braking	1.342	2.855	0.361	67.61%
300 mm	Straight	1.414	3.661	0.522	50.44%
	Cornering	1.410	3.503	0.392	49.32%
	Braking	1.342	2.838	0.404	68.64%
0 mm	Straight	1.433	3.661	0.435	50.05%
	Cornering	1.302	3.544	0.436	49.90%
	Braking	1.355	2.799	0.336	67.17%

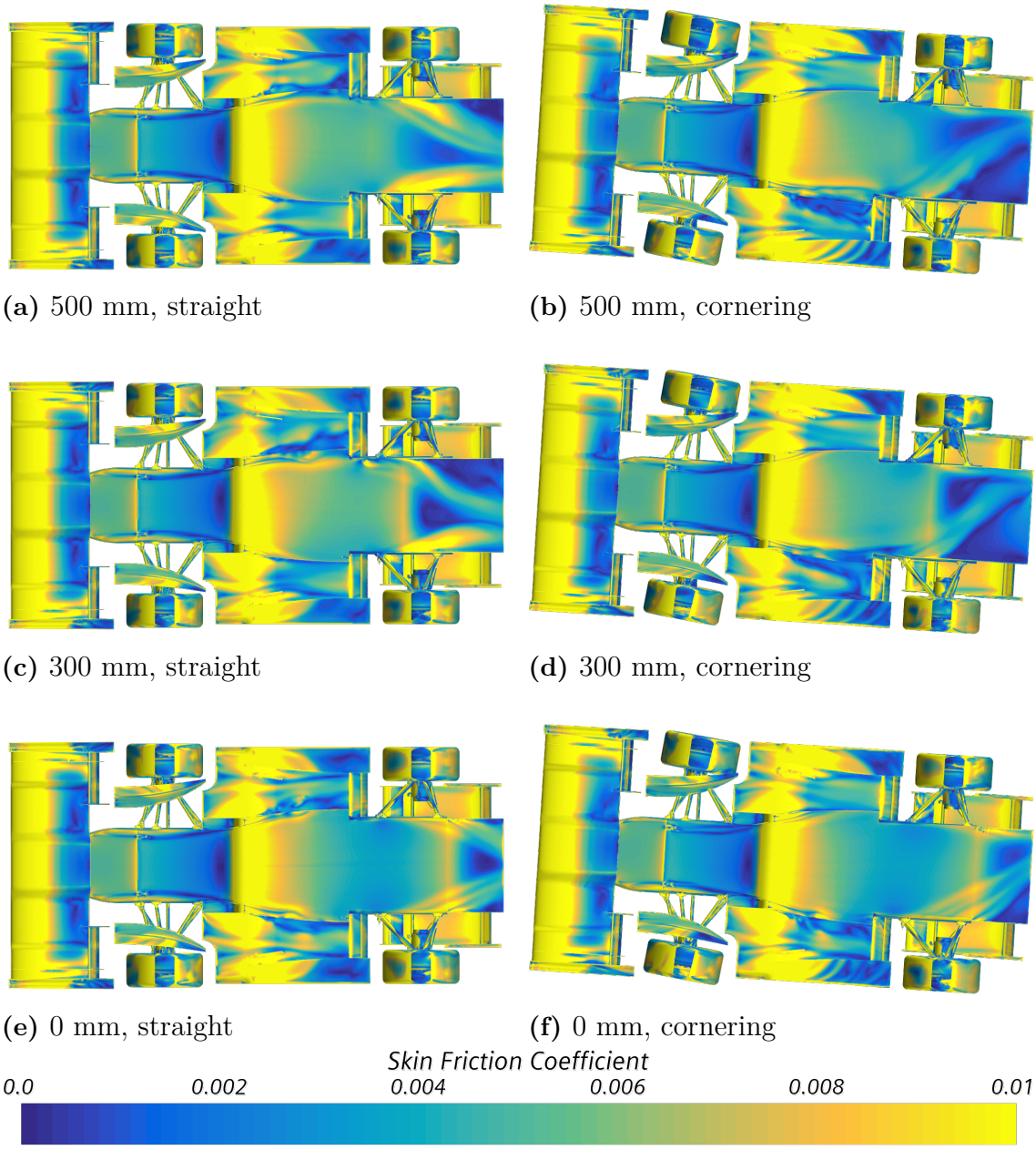

(a) 500 mm, straight

(b) 500 mm, cornering

(c) 300 mm, straight

(d) 300 mm, cornering

(e) 0 mm, straight

(f) 0 mm, cornering

Figure 4.9: Skin friction for different diffuser starting points while driving straight and during cornering.

Furthermore, the skin friction coefficient showed a more noticeable difference between all three designs. As can be seen in Figure 4.9, the biggest difference is inside the diffuser. Both the 300 mm and 0 mm designs show an increase in skin friction at the starting point of the diffuser followed by a region in the middle of the diffuser with low skin friction which can be seen in Figure 4.9c and 4.9e. The 500 mm design however created a smoother gradient in between these regions shown in Figure 4.9a which could indicate that the 500 mm design is more aerodynamically robust than the 300 mm and 0 mm case, being less prone to seperation.

In the cornering scenarios the same aforementioned phenomenon is displayed but

with the 0 mm design showing the smallest region of low skin friction in the diffuser. This was likely a result of having a smaller volume of expansion which means the air passing through the diffuser did not need to expand as much. The smaller expansion causes the diffuser to pull less air from the underfloor of the monocoque which can be seen in Figure 4.9. The underfloor of the monocoque shows better attachment for the 500 mm and 300 mm design compared to the 0 mm design.

All things considered, the 500 mm design was chosen to carry forward. Firstly, all three designs showed similar performance but with the 500 mm and 0 mm designs showing the most robust results. Secondly the 500 mm design had a larger volume than the 0 mm design which was deemed to be useful for further development.

4.3 Expansion Angle of the Diffuser

Different expansion angles of the diffuser were tested with a starting point of 500 mm from the back of the monocoque, see Figure 3.4 for visualization. The data from those simulations are found in Table 4.3. Figure 4.10 shows the skin friction for the different angles of the diffuser. As the angle increases it can be seen that the transition to the low skin friction region in the middle of the diffuser becomes more aggressive meaning that the flow detaches more drastically. The skin friction for the cornering case can be seen in Figure 4.11.

Table 4.3: Values for C_D, C_L, C_L M&D and aero balance (rearwards) for different diffuser expansion angles at the driving scenarios straight, cornering and braking.

Design	Scenario	C_D	C_L	C_L M&D	Aero balance
13°	Straight	1.419	3.729	0.515	49.68%
	Cornering	1.380	3.603	0.470	49.38%
15°	Straight	1.424	3.640	0.483	50.36%
	Cornering	1.408	3.542	0.417	49.62%
17°	Straight	1.417	3.713	0.508	49.75%
	Cornering	1.408	3.539	0.427	50.30%
19°	Straight	1.402	3.663	0.497	49.35%
	Cornering	1.417	3.567	0.418	49.54%

It is difficult to draw far-reaching conclusions from the few data points presented in the table above. The data correlating forces to the diffuser expansion angle are not monotonous, and the data points are too distantly spaced to see at which angles certain effects are introduced. However, it is evident from the final accumulated value of C_D, that the 13° diffuser is best-performing of the tested. As previously discussed in Section 2.4.1.2 this is to some extent expected due to the area ratio being around 1:5 for the 13° diffuser.

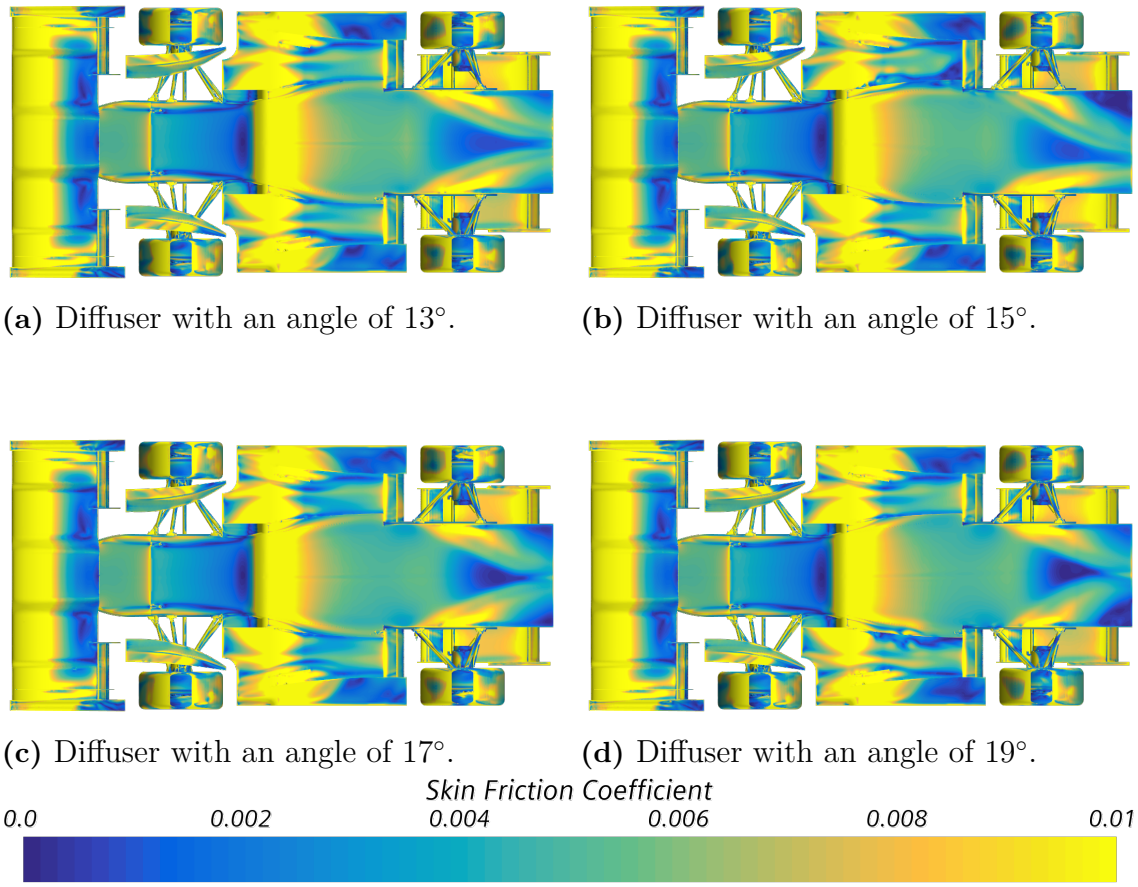

(a) Diffuser with an angle of 13°.

(b) Diffuser with an angle of 15°.

(c) Diffuser with an angle of 17°.

(d) Diffuser with an angle of 19°.

Figure 4.10: Skin friction while driving straight for diffusers with different angles.

In Figure 4.10, a correlation between the area ratio and the robustness of the vortices and overall flow in the diffuser can be identified. As seen in Figure 4.10a, the flow in a low-expansion-angle diffuser is smooth and well-attached along the length of the diffuser. An uniform low-pressure area has formed. In Figure 4.10b, the steeper angle produces vortices which are asymmetrical and detach from the surface. An irregular low-pressure area has formed, however this is difficult to distinguish from the artifacts seen in the data.

As the expansion angle increases further in Figure 4.10c and 4.10d, the flow becomes more turbulent. The vortices detach from the surface and a separation bubble has formed. The low pressure allows for backflow into the diffuser, disturbing the airstream.

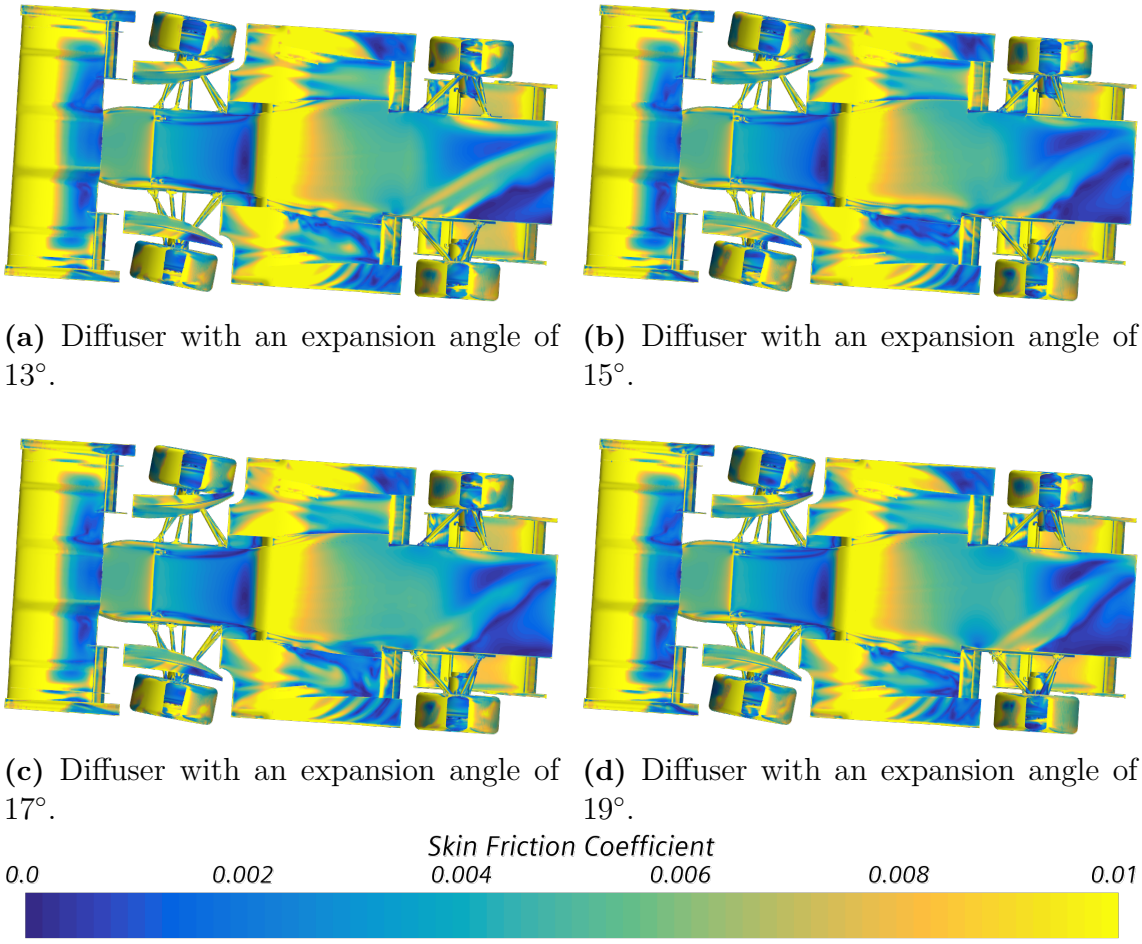

(a) Diffuser with an expansion angle of 13°.

(b) Diffuser with an expansion angle of 15°.

(c) Diffuser with an expansion angle of 17°.

(d) Diffuser with an expansion angle of 19°.

Figure 4.11: Skin friction while cornering for diffusers with different expansion angles. Note the differences in Venturi vortex generation between the different cases.

It can be seen in Figure 4.11 that the flows follow the same patterns as in the straight driving scenarios. Note the robust right vortex in the 13° and 19° diffuser, and its breakdown in the 15° and 17° diffuser. However, as is evident by the sharp borders between the vortices, flow separation has occured in the 19° diffuser. Also note the lack of the left vortex.

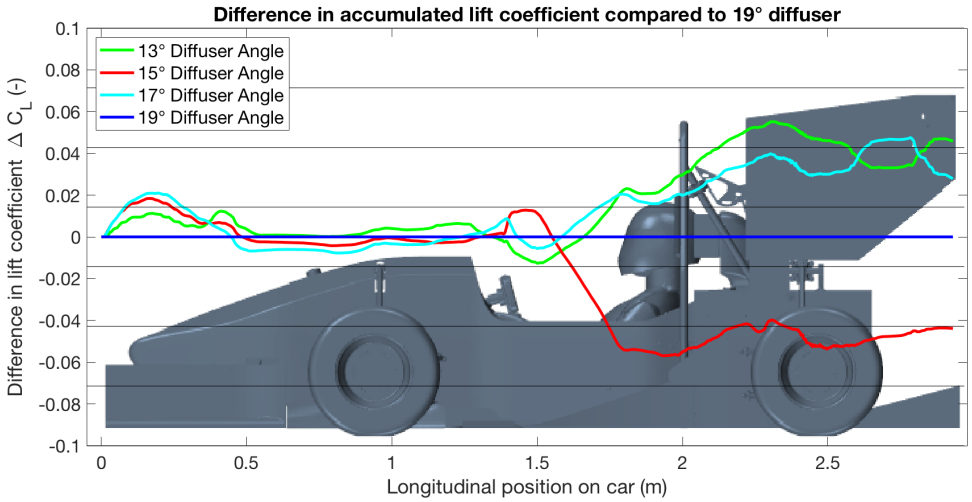

(a) Relative difference in accumulated lift coefficient for the straight driving scenario.

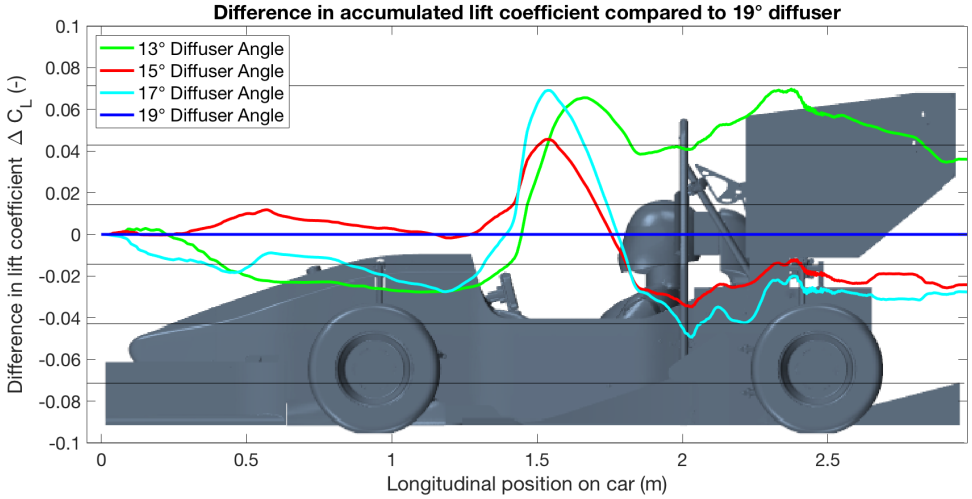

(b) Relative difference in accumulated lift coefficient for the curved driving scenario.

Figure 4.12: Difference in accumulated lift coefficient C_L, relative to the 19° diffuser for the straight and curved driving scenarios. A higher C_L implies a greater downforce.

The accumulated C_L along the length of the car clearly shows the impact of changes to the design. In Figure 4.12, the non-monotonous correlation between the diffuser expansion angle and downforce is evident. It is also clear that changes to the diffuser affect the performance of the whole underbody of the car. The case of the 17° diffuser shows that good performance for straight driving doesn't imply the same for the cornering case.

Since the 13° diffuser outperforms the other diffuser designs in terms of C_L in both scenarios, its flow seems to be more controlled and the separation bubble is less apparent, it is chosen for further development. The 19° diffuser doesn't differ much between the scenarios, in terms of C_L, and it has the second greatest C_L in cornering. It also has the largest potential in terms of area expansion and is therefore chosen

for further development.

4.4 Implementation of Strakes

Continuing the design process the two diffuser angles showing best performance, 13° and 19°, were developed further by introducing strakes. This was also done to analyze the impact of strakes on the two extreme cases in terms of angle. The results can be found in Table 4.4. Only the straight and cornering scenarios were simulated due to resource restrictions.

Table 4.4: Values for C_D, C_L, C_L M&D and Aero balance (rearwards) for 13° and 19° diffusers with and without strakes.

Design	Scenario	C_D	C_L	C_L M&D	Aero balance
13°	Straight	1.419	3.729	0.515	49.68 %
	Cornering	1.380	3.603	0.470	49.38 %
13° strakes	Straight	1.404	3.747	0.565	50.08 %
	Cornering	1.316	3.562	0.461	49.00 %
19°	Straight	1.402	3.663	0.497	49.35 %
	Cornering	1.417	3.567	0.418	49.54 %
19° strakes	Straight	1.403	3.687	0.528	50.14 %
	Cornering	1.312	3.610	0.460	49.44 %

It can be observed that the 13° diffuser is generating more total downforce compared to the 19° diffuser in the straight scenario, regardless of strakes. In the cornering scenario the downforce is largest for the 19° diffuser with strakes. Adding strakes to the 13° diffuser increases the downforce in the straight scenario but decreases it while cornering. The 19° diffuser produces more downforce with strakes in both scenarios. The aero balance moves forward slightly while cornering for all designs. Additionally, C_D is reduced during cornering if strakes are added. Overall, strakes seem to improve the performance in most cases.

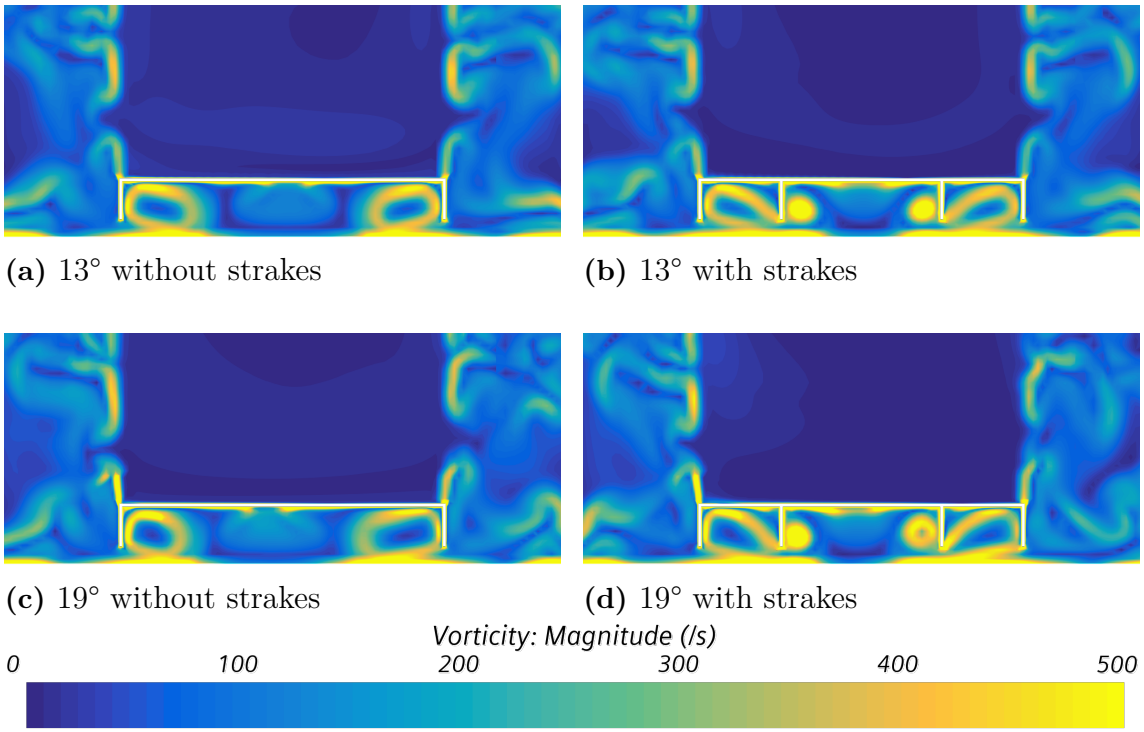

(a) 13° without strakes

(b) 13° with strakes

(c) 19° without strakes

(d) 19° with strakes

Figure 4.13: Vorticity magnitude while driving straight for the 13° and 19° diffusers with and without strakes. The visualized yz-plane cuts through the diffuser 27 mm behind the monocoque.

Vorticity magnitude plots are presented in Figure 4.13. The diffusers without strakes induce two vortices aligned with the outer walls. Implementing strakes induce four vortices, adding two within the strake walls. These help to reduce the size of the separation bubble usually formed in the middle. Furthermore, the pressure drops where the vortices are located. Vortices rotate at high velocity which in theory should increase the downforce. This pressure difference is apparent in Figure 4.14.

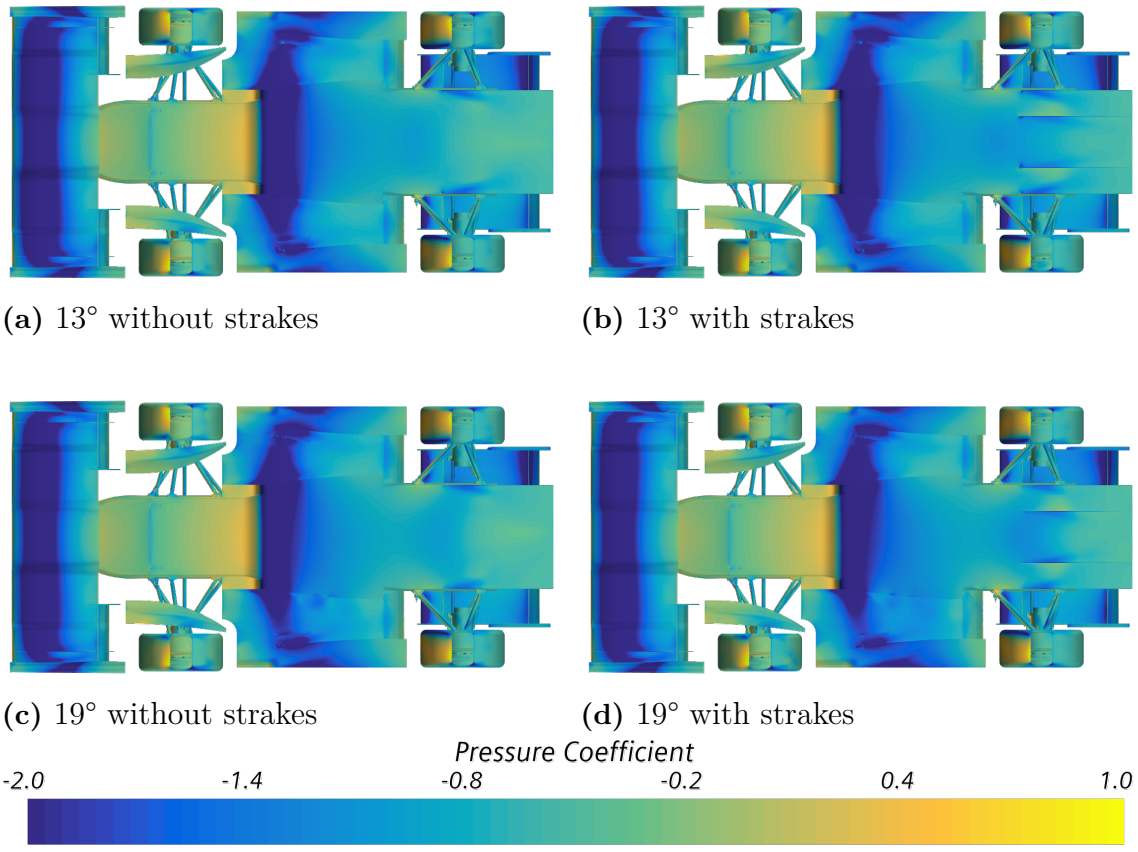

(a) 13° without strakes

(b) 13° with strakes

(c) 19° without strakes

(d) 19° with strakes

Figure 4.14: Pressure coefficient on the underside surface of the car while driving straight. The four different diffuser designs with expansion angles 13° and 19°, with and without strakes, are presented.

The pressure coefficient underneath the car is presented in Figure 4.14. As previously discussed, low pressure regions are apparent where the vortices are located for both diffuser angles. The pressure in the area between the strakes is lower when compared to designs without strakes, i.e generating more downforce. Table 4.4 reinforces this observation since C_L for M&D is significantly increased for both angles with strakes in the straight scenario.

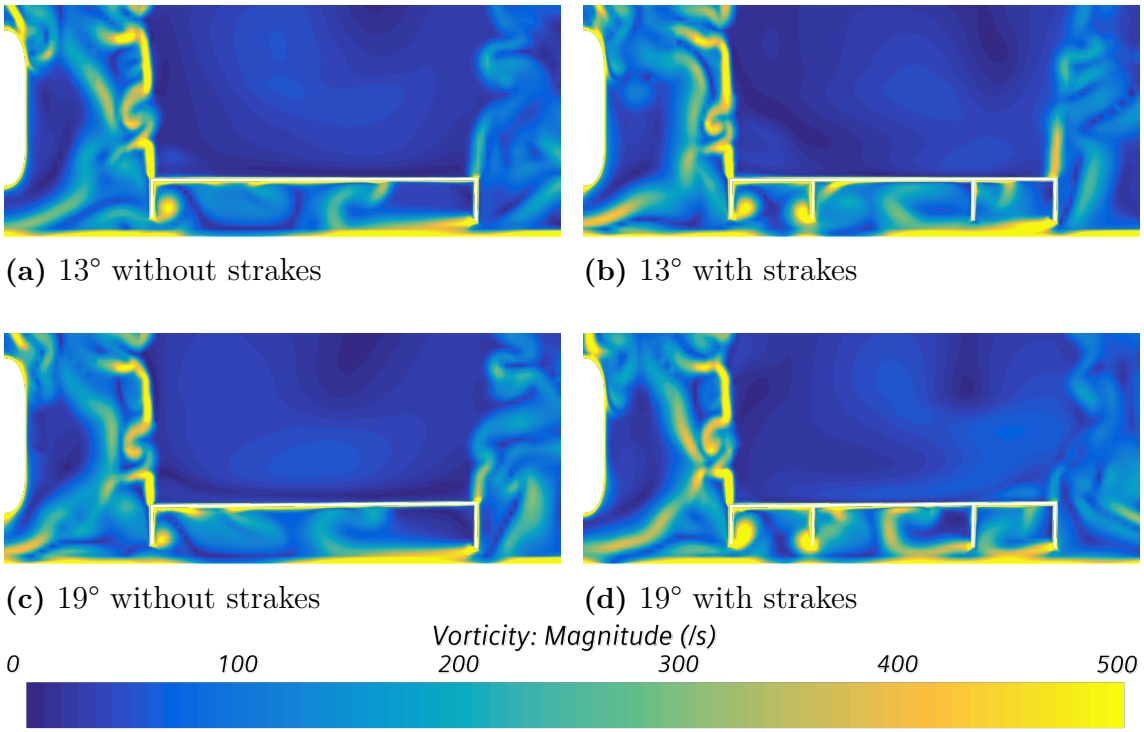

(a) 13° without strakes

(b) 13° with strakes

(c) 19° without strakes

(d) 19° with strakes

Figure 4.15: Vorticity magnitude while cornering for the four diffusers with 13° and 19° angles with and without strakes. The visualized yz-plane cuts through the diffuser 27 mm behind the monocoque.

Vorticity magnitude while cornering for the four cases is presented in Figure 4.15. Similar to the straight scenario, strakes influence the number of induced vortices in both the 13° and 19° diffusers. Two vortices are created in the left most channel, creating two low pressure stripes. Another two can be seen on the right side. These appear to break up, a phenomenon also observed without strakes. However, the separation bubble size is still reduced which is seen in Figure 4.16.

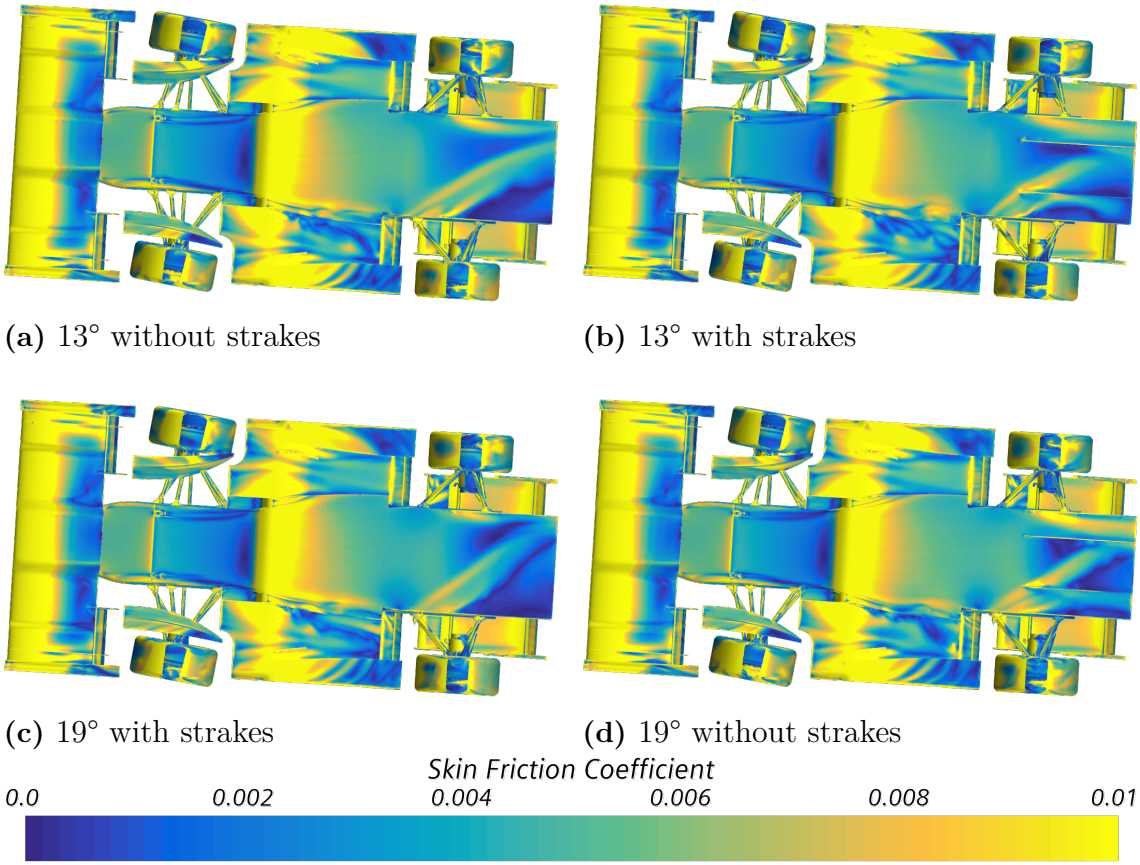

(a) 13° without strakes

(b) 13° with strakes

(c) 19° with strakes

(d) 19° without strakes

Figure 4.16: Skin friction on the underside of the car. The four different diffuser designs with expansion angles 13° and 19°, with and without strakes, are presented.

The skin friction coefficient during cornering is presented in Figure 4.16. It is clear that the strakes influence the flow pattern considerably. The main separation bubble is reduced in size due to the new vortices, especially for the 13° diffuser. Even though this particular diffuser does not perform the best in the cornering scenario, the flow seems to be the best controlled with the most attachment. This should mean that more performance is attainable with continued design development, which is investigated in the next section.

4.5 Implementation of Side Floors

Data from simulations with side floors added to the diffuser can be seen in Table 4.5. The designs that proved to perform better in the previous section, i.e. 13° and 19° with strakes, were also those who got further developed by adding side floors. By adding side floors C_L and C_L M&D increased in all cases except in the braking scenario for the 19° diffuser. The 13° diffuser has the overall best performance in the study in all scenarios. The only exception is in cornering where C_L is on par with the 19° diffuser with side floors. Additionally, the C_D performance of the 13° is the best during cornering and on par with the best diffusers in other scenarios.

Table 4.5: Values for C_D, C_L, C_L M&D and aero balance (rearwards) for 13° and 19° diffusers with and without side floors.

Design	Scenario	C_D	C_L	C_L M&D	Aero balance
13° strakes	Straight	1.404	3.747	0.565	50.08%
	Cornering	1.316	3.562	0.461	48.10%
	Braking	1.355	2.894	0.377	68.12%
13° strakes + side floors	Straight	1.409	3.854	0.647	50.93%
	Cornering	1.291	3.619	0.517	49.83%
	Braking	1.332	3.005	0.487	66.90%
19° strakes	Straight	1.403	3.687	0.528	50.14%
	Cornering	1.312	3.610	0.460	49.44%
	Braking	1.352	2.983	0.417	67.95%
19° strakes + side floors	Straight	1.405	3.767	0.583	50.21%
	Cornering	1.313	3.624	0.494	50.08%
	Braking	1.332	2.756	0.347	66.28%

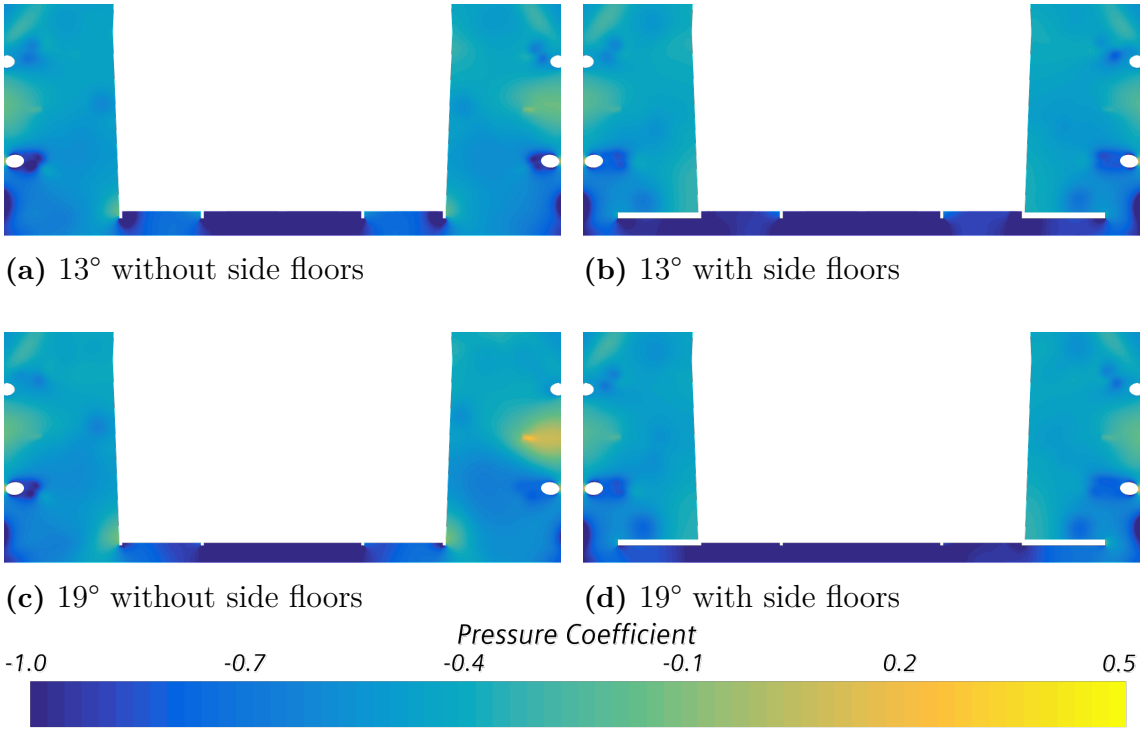

(a) 13° without side floors

(b) 13° with side floors

(c) 19° without side floors

(d) 19° with side floors

Figure 4.17: Pressure coefficient for the 13° and 19° diffusers with and without side floors while driving straight are illustrated. The visualized yz-plane cuts through the diffuser 27 mm into the back of the monocoque.

Figure 4.17 illustrates how a lower pressure can be maintained at the beginning of the diffusor as a result of adding side floors, compared to without. The side floors reduce the pressure outside the diffuser side walls, on the underside of the floors. This results in a larger low pressure area and the entire diffuser generates more

downforce, which can be seen in Table 4.5.

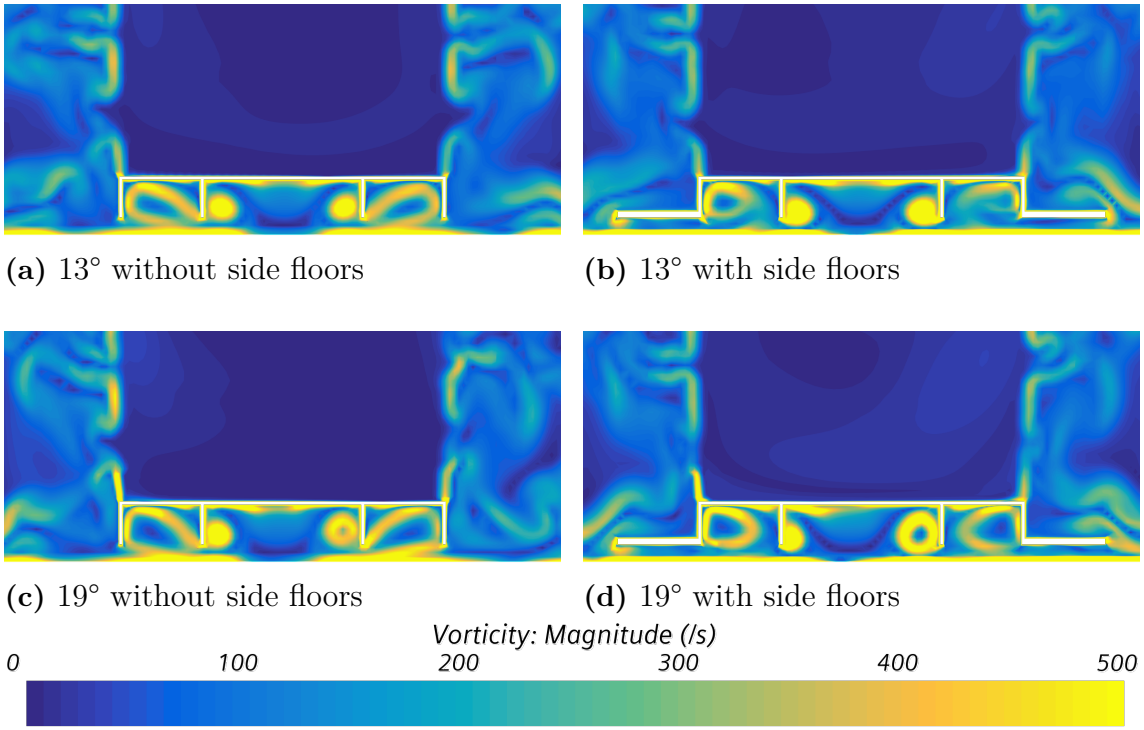

(a) 13° without side floors

(b) 13° with side floors

(c) 19° without side floors

(d) 19° with side floors

Figure 4.18: Vorticity magnitude with and without side floors while driving straight. The visualized yz-plane cuts through the diffuser 27 mm behind the monocoque.

The vorticity magnitude plots in Figure 4.18 shows that the vortices created in the side strake channels are somewhat weaker for the diffusers with side floors, compared to those without. A reason might be that the pressure is reduced under the side floors, which can be seen in Figure 4.17, and therefore level out the pressure difference on either side of the diffuser side walls. Smaller pressure difference tends to induce weaker vortices. Another cause could be that the side floors limit the air flow from the sides, limiting the available energy needed to induce vortices. However, the two inner vortices are slightly strengthened by the floor addition and overall the pressure is reduced.

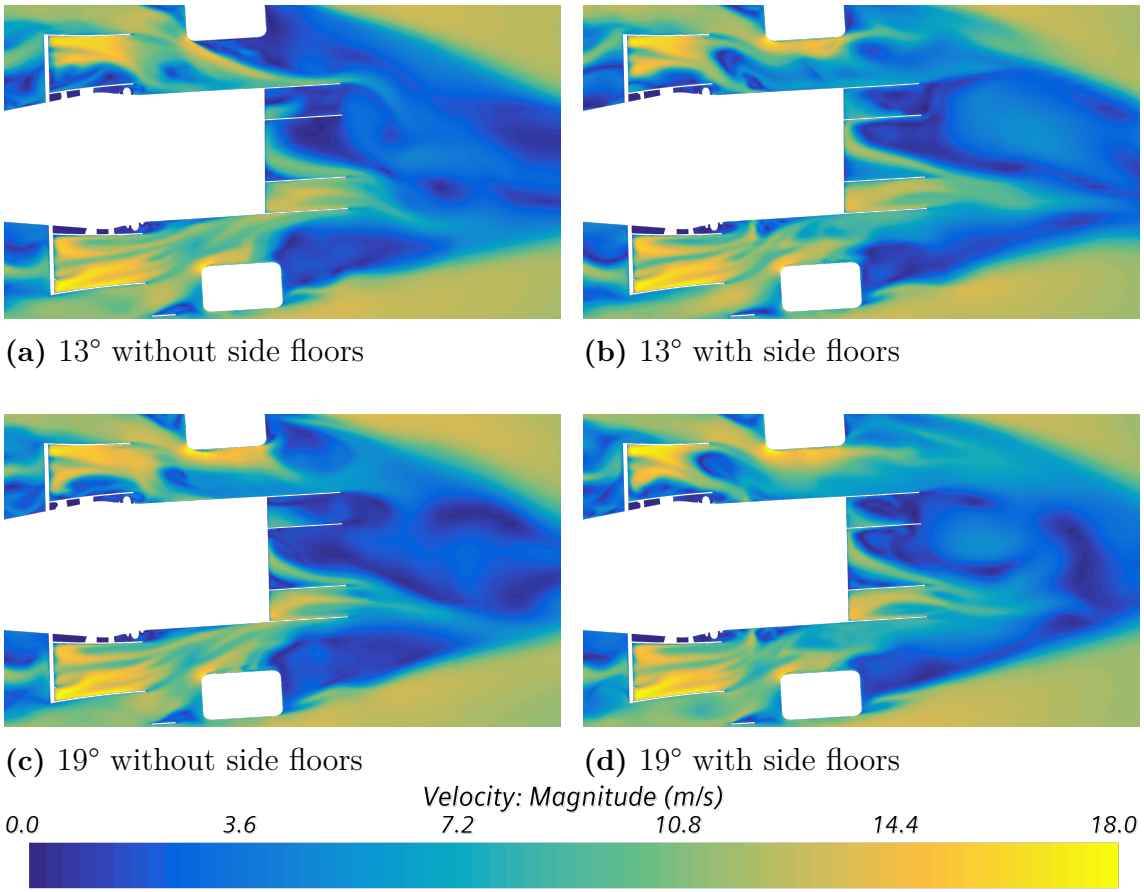

(a) 13° without side floors

(b) 13° with side floors

(c) 19° without side floors

(d) 19° with side floors

Figure 4.19: Velocity magnitude during cornering. The visualized xy-plane is located at $z = 78$ mm above ground.

An improvement to the wake management behind the rear wheels is observed with side floors added when cornering, see Figure 4.19. Figure 4.19b and Figure 4.19d illustrates that the wakes created behind the tires are to some extent prevented by the side floors from entering the diffuser and interfering with the surrounding air. Since the tire wake is turbulent and could have a negative effect on the diffuser performance if it gets too close, managing it should in theory improve the predictability and performance of the diffuser.

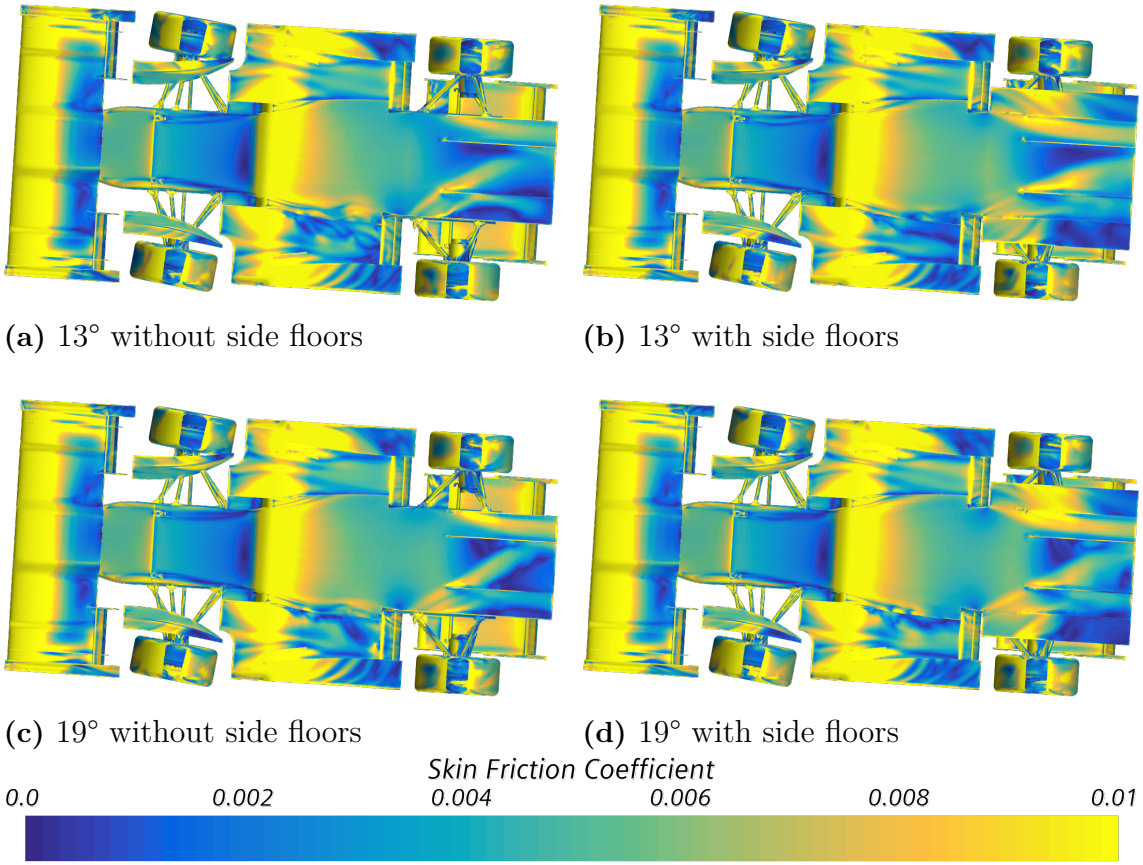

(a) 13° without side floors

(b) 13° with side floors

(c) 19° without side floors

(d) 19° with side floors

Figure 4.20: Skin friction under the car with and without side floors while cornering.

Figure 4.20 shows how the skin friction coefficient is affected by the addition of side floors. Adding side floors seem to improve attachment for both angles, especially for the 13° design. Similarly to the straight scenario in Figure 4.18, the vortices in the middle channel are larger and better attached. The 13° diffuser with side floors, which performed the best overall according to Table 4.5, seems to have more attachment of the flow compared to the 19° diffuser with side floors. This can be seen mainly in the middle and left most channel of the diffuser (i.e. the channel at the top of the figure) and could explain why the drag force is larger for the 19° diffuser. However, the downforce is similar for the two designs.

4.6 Summary

In summary, the best performing diffuser design is the 13° with strakes and side floors. Comparing this to the small 0 mm baseline diffuser shows significant improvements. The results can be seen in Table 4.6 are further discussed in Section 5.1.

Table 4.6: Values for C_D, C_L, C_L M&D and aero balance (rearwards) for different driving scenarios comparing the small 0 mm diffuser and the best performing 13° diffuser with strakes and side floors.

Design	Scenario	C_D	C_L	C_L M&D	Aero balance
Small 0 mm	Straight	1.433	3.612	0.435	50.06%
	Cornering	1.302	3.544	0.436	49.90%
	Braking	1.355	2.799	0.336	67.17%
13° strakes + side floors	Straight	1.409	3.854	0.647	50.93%
	Cornering	1.291	3.619	0.517	49.83%
	Braking	1.332	3.005	0.487	66.90%

5
Discussion

In this chapter several subjects are discussed. Firstly, vehicle dynamics and the impact of the new diffuser are considered. Secondly, the implications on other subsystems of the car are explored. Lastly, the method and its inherent errors are reviewed.

5.1 Impact on Vehicle Dynamics

This section discusses the results from a vehicle dynamics point of view.

5.1.1 Vehicle Dynamics While Cornering

The results from simulations using the best performing diffuser, the 13° diffuser with strakes and side floors, indicate that the aerodynamic characteristics of the car change slightly when comparing the straight and cornering scenarios. See Table 4.6. The downforce while cornering is approximately 6% lower than while driving straight, showing that the aerodynamic package design is not optimized for cornering. This is no surprise since every component except for the diffuser has been developed using only half-car straight simulations. The balance however remains approximately the same at around 50% which demonstrates that there is no significant balance shift when entering a corner. This consistency is in general preferred in a racing car.

The pressure distribution (similar to Figure 4.5c) shows that the low pressure region in the middle of the car is asymmetric, being shifted to the left and inner side of the car. The aerodynamic load is therefore larger on the inside wheels. The normal force on the outside wheels are naturally larger during cornering due to the vehicle mass inertia. The aerodynamic load counteracts this slightly, distributing the load more evenly across the four tires. This could be beneficial for the balance of the car and to even out the tire wear. The diffuser is not the only contributing factor since the complete aerodynamic package is affecting the flow.

The 13° diffuser improved downforce during cornering by approximately 2% compared to the small diffuser design. Consequently, slightly higher cornerning speeds should be possible to maintain. Additionally, the 13° diffuser improve the generated downforce by 7% when driving straight. C_L M&D improved significantly in both cases, by 49% in straight and 19% during cornering, showing that the downforce

generated by the diffuser and monocoque is contributing heavily to the improvements.

The aero balances are approximately the same for the two designs during cornering. There is one percentage point difference of aero balance shift between straight and cornering when comparing the two designs, the 13° diffuser shifting by 2% compared to 1%. If this effect is not a result of inaccuracies in the simulations, the 13° diffuser could produce marginally more volatile balance changes between driving straight and cornering compared the small diffuser design.

5.1.2 Vehicle Dynamics While Braking

Locking the brakes is preferably avoided during racing. If not, the lap times increase and the tires might be damaged. Increased load on the tires makes it possible to produce larger braking forces without locking up. In addition, it is desirable for the downforce distribution to be sustained while braking, reducing any radical balance shift. Unfortunately, as seen in Table 4.6, the downforce and balance change dramatically during braking. C_L drops by 22 % for the 13° diffuser and 24 % for the small diffuser. Even though neither design is assuring great aerodynamic robustness, the larger 13° diffuser performs better.

The large decrease in downforce for the front wing (43 % for both designs) leads to a signficant shift in the aero balance from approximately 50% rearwards while driving straight or cornering to 67% while braking. This could result in the braking procedure becoming more intricate for the driver. The decrease of front aerodynamic load might promote locking of the front tires. However, due to the mass of the car, the load on the tires is already heavily shifted forwards during braking. The aero balance shift backwards counters this somewhat, reducing the total balance shift experienced by the driver and potentially even increasing the predictability of the car. Furthermore, front wheel locking is preferable to rear wheel locking since the latter might cause the car to spin. The aero balance shift backwards may therefore aid in reducing the risk of spinning.

The aero balance shift is slightly smaller for the 13° diffuser compared to the small diffuser and it could therefore be deemed the most stable of the two. However, this difference is very small and is not expected to affect the car's dynamics significantly. Conversely, the total downforce generated is 7 % larger for the 13° diffuser. This indicates a considerable improvement compared to the small diffuser.

5.1.3 Summary

In summary, the new and improved 13° diffuser design shows better performance in every simulated driving scenario compared to the small diffuser. These improvements are believed to result in a car that is easier to control and that can produce

better lap times.

5.2 Implications of a New Diffuser on the Car's Subsystems

In this section the implications of a new and larger diffuser on the car and its subsystems are discussed.

5.2.1 Implications on Non-aero Vehicle Subsystems

The back of the monocoque contains components of the car's powertrain such as the battery. An earlier starting point of the diffuser leads to less space for the powertrain components and a rearrangement of the components might not be feasible. In this report these considerations have been secondary but it should be noted that there are limitations in how much of the monocoque that can be re-shaped.

Worth noting is that the center of gravity is elevated with the larger 13° diffuser compared to keeping the monocoque flat with a smaller diffuser. The battery and other powertrain components would have to be raised or slanted, moving their center of gravity's upwards. This would in general affect the vehicle dynamics negatively. It is however important to realize that the design is far from optimized. Continuing development within CFS of the already well performing 13° diffuser is thought to result in significant aerodynamic performance gains and as a result lap time improvements. This could make it worthwhile to construct a new diffuser and monocoque.

5.2.2 The Diffuser's Synergy with the Aero Package and Possible Changes

The benefit of the diffuser is that it is located at the back of the car which leads to it not creating significant changes to other aerodynamic components unlike for example the front wing. The component which intuitively should be most impacted when changes to diffuser is made is the side wings. However, the results seem to indicate that the side wings are marginally affected in terms of downforce from changes to the diffuser, see Appendix A.1. So perhaps this is an area where improvement can be done. Creating more synergy between the diffuser and the side wings might lead to downforce increases. One concept to make this possible could be to integrate the side floors more with the side wings to get rid of the early area of high pressure of side floors, see Appendix A.2, Figure A.1b.

Changing the front wing can have major effects on the diffuser. The front wing dictates a big part of the mass flow under the floor of the car. By changing the angle of attack of the front wing's airfoils the mass flow under the floor changes. A smaller angle of attack might decrease the front wing's downforce but the loss can neutralized by the expected increase in downforce of the diffuser. The opposite change can be made if it is believed that the diffuser can handle a lower mass flow.

This might lead to a decrease in the diffuser's downforce but an increase in the front wing's downforce. A caveat here is that the aero balance of the car should also be taken in to account when changes to the front wing is made. Increased front wing downforce will lead to a more front biased aero balance while decreased front wing downforce will lead to a more rear biased aero balance.

Moving the step of the floor longitudinally can also be an optional change. There is a region of very low pressure directly after the step of of floor as can be seen in Figure 4.5. This region is the major contributor to the downforce that the diffuser creates. The pressure coefficient then increases but is still negative for the rest of the floor. The region after the low pressure region should still be a contributor to the downforce although it is minor compared to the low pressure region. Perhaps there is a possibility to increase the area of this region while still maintaining the same area of the low pressure region by moving the step forward, thus increasing the downforce. A side effect of this configuration is that the aero balance will move forward because of the low pressure region moving forward.

There is also a possibility in utilizing the radiator system's fans. The current CFS car has fans placed on the diffuser, as mentioned in Section 3.1.1, to "pump" out more air in the diffuser while cooling the car with the radiators. Implementing a similar system would enable a larger diffuser angle and therefore a larger area ratio. This might lead to an increase in downforce. A possible difficulty that might arise is simulating the behavior of the fan and radiator in Star-CCM+.

5.3 Comments on Methodology

The simulations have both systemic and arbitrary sources of inaccuracy. These inaccuracies are discussed in this section.

5.3.1 Whole-car Versus Half-car Simulations

This project has used a whole-car for all simulations. This was necessary to get comparable results among the driving scenarios since cornering can not utilize half-car symmetry. This also led to the results likely being more accurate since some phenomenons like vorticies are sensitive to surrounding flow patterns. However, the simulations took approximately twice as long to perform and comparison of the results with former work done by CFS could not be made since all their data comes from half-car simulations. A thorough study of how half and whole-car simulations correlates would ease this in future work.

5.3.2 Cornering Left and Right

During the cornering simulations performed in this project, the car was always simulated turning left. The main reason for this was that it was assumed that both left and right turns would give the same result. This was never properly validated in this project but earlier studies performed by CFS has shown there is little to

no difference in which way the car is turning [7]. This is however suggested to be fully validated in future work to ensure that the cornering performance is consistent regardless of turning direction.

5.3.3 Mesh Inaccuracies

This project contained no thorough study of the simulation's mesh because of time limitation. This means that the results might not be mesh independent. However, since the mesh is a slightly finer version of CFS's mesh it should still be considered relatively reliable. A simulation with the exact same mesh gave the same results. Two simulations which were meshed separately with the same mesh settings gave a difference in C_L and C_D of $< 1.5\%$ compared to each other.

C_D and C_L are therefore prone to having inaccuracies even though they are created with a mean of the last 500 iterations of a simulation. Therefore, if two case's lift coefficient only differ 0.02 between each other one should not be considered better than the other. That is why a lot of the analysis is based on comparing figures of the quantities of the air flow. A diffuser which generates slightly lower downforce can therefore still be deemed better if the figures seem to show better results.

5.3.4 Approximation of Center of Rotation for Roll and Pitch

The center of pitch and roll used in this project is located at the center of mass of the car. This approximation had to be made since the CFS suspension subgroup had no available data of where the actual centers were located. The results might therefore be slightly wrong but since the angles used are small (1° for the pitch angle and 0.7° for the roll angle) there should not be much difference between using the correct centers and the center of gravity.

5.3.5 Mean of Fields

Fields of quantities, such as skin friction or velocity magnitude, which are shown in figures are not averaged over the last 500 iterations. It was realized too late that fields has to be averaged. This means that the fields shown in figures are momentary, only showing the last iteration of the fluctuating but steady solution. Drawing conclusions from regions where oscillating turbulence exists should therefore be done with caution.

This problem could be solved by adding monitors for the mean pressure and velocity. These monitors create a mean of the last 500 iterations. Coefficients, such as the pressure coefficient, can be calculated using the monitors with field functions and be displayed as the mean of the last 500 iterations.

5.3.6 No Wind Tunnel Validation of the Data

Since this study is entirely computer based because of limited resources there is no wind tunnel validation. This leads to a fundamental unreliability in the results for the reason that physical data can not confirm that the CFD results are correct. However, CFS18, who used a similar setup as used in this work, performed a wind tunnel test which showed that CFD overestimates downforce with only 6.1% which somewhat reassures the results [16].

6
Conclusion

This chapter summarizes the project and gives suggestions on what can be further investigsated within the subject.

6.1 Description of The Final Design Proposal

Given the results and analyses performed in this project, a final design concept has been developed. The concept consists of a diffuser with the following design:

- A starting point 500 mm from the monocoque's back
- An angle of 13°
- Two strakes
- Side floors

A starting point 500 mm from the monocoque's back resulted in the least amount of separation compared to the other starting points. With 500 mm, a smoother skin friction gradient in the diffuser was obtained. An angle of 13° proved to perform best from the selection of angles tested. The 13° diffuser had the most downforce and flow attachment. Adding strakes showed that the overall performance was improved. With the additional vortices created from the strakes there was more attachment of the flow resulting in an increase of downforce. Finally, adding side floors, the 13° diffuser performed the best in all driving scenarios.

In comparison with the reference, i.e. the mini diffuser introduced in Section 4.1, the final concept performs better. For all driving scenarios, higher downforce and lower drag force are obtained. The concept developed has thus fulfilled the project's purpose of increasing the aerodynamic performance of the car and it is recommended to continue the development in this direction.

6.2 Final choice of Simulated Driving Scenarios

From the method it was found that the following driving scenarios were the most critical when it comes to aerodynamics, and specifically downforce:

- Driving straight ahead
- Braking

- Cornering

As mentioned in Section 3.3.2, driving straight ahead is included both to provide a basic understanding of diffusers and to enable comparison with previous diffuser designs from CFS. Cornering and braking are frequent maneuvers during a race, and are therefore chosen to be implemented in the design process. When cornering, which is clarified in Section 3.3.3, the car behaves differently due to the body slip, steering, and roll angle. During braking, a rotation occurs with a pitch angle which affects the flow around the car. Among other things, it is proven that the car's aero balance is significantly affected by the braking. To ensure that a diffuser design is aerodynamically robust, these three driving scenarios were therefore implemented in simulations.

6.3 Recommendations for Further Research

For further research, a wider diffuser could be tested to increase the absolute volume so that the air can expand even faster and generate a faster flow under the car. It might also be interesting to investigate how the car would be affected by a diffuser that is gradually widened. In this project, the diffuser has only been widened in the z-direction and therefore it would be of interest to try to widen the diffuser in the y-direction.

Furthermore one could experiment with the vortices generated in the diffuser in order to create low pressure areas in the diffuser. In this project, it has been shown that vortices can cause more attachment of the flow in the diffuser. For further development, it would therefore be of interest to try a larger number of strakes as well as strakes of different sizes and positions.

The side floors are also an area that could be beneficial to analyze further. It would be interesting to try different widths, unlike this project which only had time to try one. There is plenty of space left to use, based on what is allowed according to the Formula Student regulations. However, the impact on the suspension needs to be taken into consideration.

Bibliography

[1] Chalmers Formula Student. "Formula student," Chalmers Formula Student, [Online]. Available: http://www.chalmersformulastudent.se/formula-student/ (visited on 04/22/2021).

[2] The Editors of Encyclopaedia. "Automobile racing," Britannica.com, [Online]. Available: https://www.britannica.com/sports/automobile-racing (visited on 04/22/2021).

[3] J. Katz, *Race Car Aerodynamics: Designing for Speed*. Massachusetts, MA, USA: Bentley Publishers, 1995.

[4] G. Piola, "Banned: The full story behind brabham's f1 fan car," *Motorsport.com*, Oct, 7, 2020. [Online]. Available: https://us.motorsport.com/f1/news/banned-tech-brabham-bt46b-fan/4808235/?nrt=54 (visited on 04/20/2021).

[5] *Formula student rules 2022*, version 0.9, Langenhagen, Deutschland. [Online]. Available: https://www.formulastudent.de/fileadmin/user_upload/all/2022/rules/FS-Rules_2022_v0.9.pdf (visited on 05/12/2021).

[6] M. Urquhart, "CFS report 2015," unpublished.

[7] L. Sobieraj, "Final report CFS20," unpublished.

[8] F. M. White, *Fluid Mechanics*. New York, NY, USA: McGraw Hill Higher Education, 2016.

[9] The Editors of CFD Online. "Finite volume," CFD Online, [Online]. Available: https://www.cfd-online.com/Wiki/Finite_volume (visited on 04/22/2021).

[10] W. Frei, "Which turbulence model should i choose for my cfd application?" *Comsol.com*, Jul. 2017. [Online]. Available: https://www.comsol.com/blogs/which-turbulence-model-should-choose-cfd-application/ (visited on 05/03/2021).

[11] F. Menter, "Two-equation eddy-viscosity turbulence modeling for engineering applications," *AIAA Journal*, pp. 1598–1605, 1994.

[12] B. Jacobson, *Vehicle Dynamics - Compendium for Course MMF062*. Gothenburg, Sweden: Chalmers University of Technology, 2015.

[13] A. Ruhrmann and X. Zhang, "Influence of diffuser angle on a bluff body in ground effect," *Journal of Fluids Engineering-transactions of The Asme - J FLUID ENG*, vol. 125, Mar. 2003. DOI: 10.1115/1.1537252.

[14] A. Berndtsson, R. Hagvall, E. Josefsson, F. Ljungqvist, M. Persson and L. Roos, "Numerisk beräkning av luftmotstånd på en personbil vid kurvtagning," Chalmers University of Technology, Gothenburg, Sweden, Jun. 2017.

[15] R. Hagvall, E. Josefsson, S. Sebben and M. Urquhart, "Numerical analysis of aerodynamic impact on passenger vehicles during cornering," May 2018. DOI: 10.4271/2018-37-0014.
[16] E. Josefsson, "CFS REPORT 2018," unpublished.

A

Appendix 1

A.1 Lift Coefficient for Side Wings

Table A.1: The side wings' lift coefficient for all the straight simulations

Diffuser type	C_L side wings
0 mm 15°	0.862
300 mm 15°	0.813
500 mm 13°	0.881
500 mm 15°	0.826
500 mm 17°	0.885
500 mm 19°	0.865
500 mm 13° strakes	0.872
500 mm 19° strakes	0.869
500 mm 13° strakes, side floors	0.879
500 mm 19° strakes, side floors	0.862

Table A.2: The side wings' lift coefficient for all the cornering simulations

Diffuser type	C_L side wings
0 mm 15°	0.882
300 mm 15°	0.851
500 mm 13°	0.928
500 mm 15°	0.852
500 mm 17°	0.859
500 mm 19°	0.881
500 mm 13° strakes	0.880
500 mm 19° strakes	0.915
500 mm 13° strakes, side floors	0.894
500 mm 19° strakes, side floors	0.900

A.2 Pressure Coefficient for Diffusers with and without Side Floors

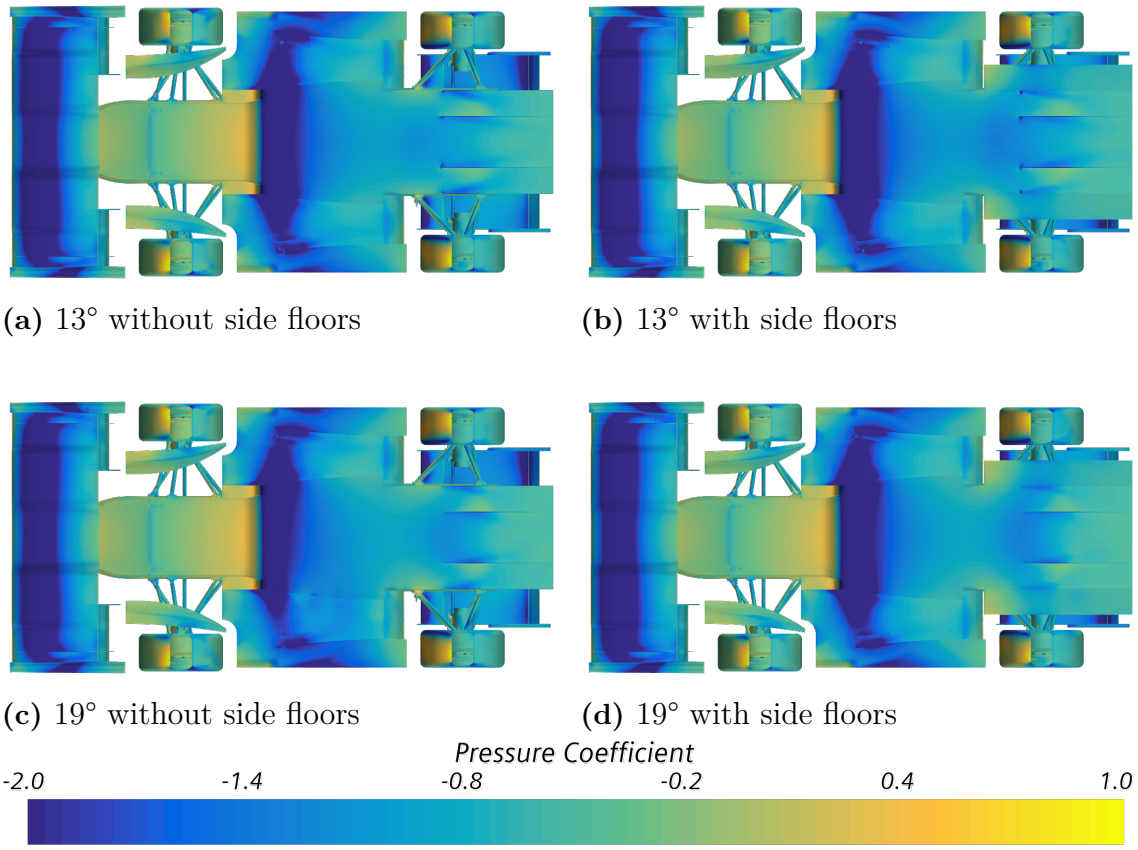

(a) 13° without side floors

(b) 13° with side floors

(c) 19° without side floors

(d) 19° with side floors

Figure A.1: Pressure coefficient under the car with and without side floors while driving straight.

DEPARTMENT OF MECHANICS AND MARITIME SCIENCES
CHALMERS UNIVERSITY OF TECHNOLOGY
Gothenburg, Sweden
www.chalmers.se

CHALMERS